JOURNAL OF PETROLOGY | VOLUME 44 | NUMBER 11 | PAGES 1937–1960 | 2003 | DOI: 10.1093/petrology/egg065

Prograde Metamorphic Assemblage Evolution during Partial Melting of Metasedimentary Rocks at Low Pressures: Migmatites from Mt Stafford, Central Australia

R. W. WHITE[1]*, ROGER POWELL[1] AND G. L. CLARKE[2]

[1]SCHOOL OF EARTH SCIENCES, UNIVERSITY OF MELBOURNE, VIC. 3010, AUSTRALIA

[2]SCHOOL OF GEOSCIENCES, UNIVERSITY OF SYDNEY, N.S.W. 2006, AUSTRALIA

RECEIVED SEPTEMBER 12, 2002; ACCEPTED APRIL 25, 2003

The Mt Stafford area in central Australia preserves a low-pressure greenschist- to granulite-facies regional aureole. The metasedimentary sequence has been divided into five zones from greenschist (Zone 1) to granulite facies (Zone 4) and a zone of hybrid diatexite formed from the introduction of granitic magma into the high-grade migmatites (Zone 5). Melt production was dominated by a series of multivariant biotite breakdown reactions, not the univariant reactions suggested by previous studies. Although the three main metasedimentary rock types produced similar amounts of melt at the highest grades, their melt production histories differed markedly as a function of temperature. Aluminous metapelites produced more melt at lower temperatures (Zones 2 and 3), whereas metapsammite and cordierite granofels experienced an additional major melt-producing step at higher temperatures (upper Zone 3 and Zone 4). This melting step involved the breakdown of biotite to produce garnet, K-feldspar and melt, and in some rocks the production of orthopyroxene. Melt production in Zone 4 exceeded 25 mol %, resulting in the formation of in situ *diatexites. Complex relationships involving aluminosilicate porphyroblasts resulted in the breakdown of biotite and aluminosilicate being drawn out over a wide temperature range, from subsolidus conditions to temperatures close to 750°C. Initially, much of the melting developed around the aluminosilicate porphyroblasts during the breakdown of coexisting biotite, aluminosilicate and quartz. However, much of the rock was chemically isolated from the porphyroblasts and could not react to produce melt. As temperatures rose, the presence of the large isolated aluminosilicate porphyroblasts controlled the spatial development of quartz-absent, spinel-present compositional domains, the formation of spinel being governed by the silica-undersaturated breakdown of coexisting biotite and aluminosilicate.*

KEY WORDS: *NCKFMASHTO; metapelite; granulite facies; petrogenetic grid; partial melting; THERMOCALC*

INTRODUCTION

In this paper we investigate the mineral assemblage and textural development of metasediments during partial melting of low-pressure upper-amphibolite- to granulite-facies metapelitic and metapsammitic rocks at Mt Stafford in central Australia. The textural, mineralogical, and partial melting evolution of these rocks is investigated by integrating textural observations with a series of calculated pseudosections.

Dehydration melting, involving the breakdown of hydrous minerals, is inferred to be the main melt-producing process that operates in the crust (e.g. Thompson, 1982; Vielzeuf & Holloway, 1988; Brown, 1994; Brown *et al*., 1995; Gardien *et al*., 1995; White *et al*., 2001). The partial melting of metapelitic and metapsammitic rocks has been the focus of numerous field (e.g. Vernon *et al*., 1990; Harte *et al*., 1991; Hand & Dirks, 1992; Fitzsimons, 1996; Carson *et al*., 1997; Sawyer *et al*., 1999; Sawyer, 2001), geochemical (e.g. Wickham, 1987; Sawyer, 1987, 1999; Greenfield *et al*., 1996), experimental (e.g. Thompson, 1982; Vielzeuf & Holloway, 1988; Carrington & Harley, 1995; Gardien

*Corresponding author. Telephone: +61 3 8344 6540. Fax: +61 3 8344 7761. E-mail: r.white@earthsci.unimelb.edu.au

et al., 1995) and petrogenetic–thermodynamic (e.g. Grant, 1985; Powell & Downes, 1990; Greenfield *et al.*, 1998; Spear *et al.*, 1999; White *et al.*, 2001) studies. These studies have shown that substantial melt can be produced in crustal rocks at high temperatures and that this melt has the potential to segregate, and in most examples migrate from the source (Brown, 1994; Brown *et al.*, 1995; White & Powell, 2002).

The prograde reactions commonly inferred to produce granulite-facies mineral assemblages are also those that produce substantial amounts of melt in the crust. Thus, high-grade mineral equilibria relationships govern the melting process (Spear *et al.*, 1999; White *et al.*, 2001). In medium- and high-pressure granulites, both muscovite and biotite melting reactions occur with rising temperature (Thompson, 1982; Brown, 1994; Spear *et al.*, 1999; White *et al.*, 2001). In contrast, muscovite breakdown commonly occurs at subsolidus conditions in low-pressure granulites (e.g. Vernon *et al.*, 1990; Brown, 1994; Brown *et al.*, 1995; White *et al.*, 2001) and melting reflects a series of biotite breakdown reactions. Despite the smaller number of melting reactions in low-pressure granulites, they may develop substantial amounts of melt (Greenfield *et al.*, 1996; White *et al.*, 2001). This high melt productivity stems primarily from the production of melts with a relatively low water content in comparison with those at higher pressure (Holtz & Johannes, 1994; White *et al.*, 2001). Partial melting at low-pressure conditions reflects perturbed crustal geotherms (e.g. Sandiford & Powell, 1991; Sandiford *et al.*, 2002). In many examples, high-T, low-P terranes are areally restricted and preserve evidence of a pronounced lateral thermal gradient outward from a high-grade core [e.g. Laramie Complex (Grant & Frost, 1990), Mt Stafford (Vernon *et al.*, 1990; Greenfield *et al.*, 1996) and Cooma (Vernon, 1982; Ellis & Obata, 1992)]. Such rocks have commonly been referred to as regional aureoles (White *et al.*, 1974). However, a discrete heat source is not always exposed at the surface.

MT STAFFORD

Regional setting

Mt Stafford occurs in the Anmatjira–Reynolds Range area of the Proterozoic Arunta Inlier of central Australia. This area is dominated by amphibolite- to granulite-facies metamorphic rocks and large volumes of deformed granitoids (Stewart, 1981; Warren, 1983), which record a complex polymetamorphic history.

The Mt Stafford area is dominated by metamorphosed turbidites of the *c.* 1870 Ma Lander Rock Beds (Blake & Page, 1988; Compston, 1995). Smaller amounts of calc-silicate gneiss, mafic gneiss and deformed and undeformed granite intrusions also occur. Peak metamorphism at Mt Stafford occurred during a pre-1820 Ma D_1–M_1 event (Collins & Williams, 1995), which was divided into D_{1a} and D_{1b} by Vernon *et al.* (1990). The area preserves only limited effects of a D_2–M_2 event that pervasively recrystallized rocks in the Mt Weldon area further east (Clarke *et al.*, 1990). The results of U–Pb dating of zircon from syntectonic granitoids were used to infer that the D_2–M_2 event was short lived and occurred between *c.* 1780 and 1770 Ma (Collins & Williams, 1995). However, the results of recent U–Th–Pb dating of zircons and monazites from granulite-facies metasediments have been used to argue that D_2–M_2 occurred at *c.* 1600 Ma (Vry *et al.*, 1996; Williams *et al.*, 1996). At Mt Stafford, the D_1–M_1 event resulted in a low-P/high-T regional aureole (Collins & Vernon, 1991), which has been divided into five zones (Greenfield *et al.*, 1996), ranging from greenschist (Zone 1) to granulite facies (Zones 4 and 5) over a distance of 10 km (Fig. 1).

Field relationships

The majority of the Mt Stafford area consists of aluminous metapelite, interbedded with metapsammite layers and cordierite granofels on a centimetre to metre scale. The cordierite granofels is inferred to be derived from siltstones that lack the stratification and other sedimentary structures common in the metapsammites. Doleritic sills intruded the metasediments, and were metamorphosed to greenschist-facies assemblages in Zone 1 and to two-pyroxene granofels in and above Zone 3. In Zone 4, these rocks were also partially melted to produce coarse-grained segregations of orthopyroxene and plagioclase. The term 'bedded migmatite' was used by Greenfield *et al.* (1996) to describe a rock unit formed from interbedded metapsammite and metapelite that dominates the outcrop at Mt Stafford. At high metamorphic grades, this rock is composed of metapelite layers that were extensively melted and metapsammite layers that are inferred to have undergone less melting. Otherwise, our migmatite terminology is based on that of Mehnert (1968), Brown (1973) and Pattison & Harte (1988). Leucosome is preferentially developed in metapelitic layers, and migmatite classifications of mesoscopic textures shown by this unit vary with grade. In Zone 2, bedded migmatite may contain metatexite (Brown, 1973), with leucosome networks filling extensional structures in metapelite layers or nebulitic migmatite, with leucosomes occurring as isolated patches homogeneously distributed throughout the metapelite layers, depending upon the intensity of D_{1a} strain.

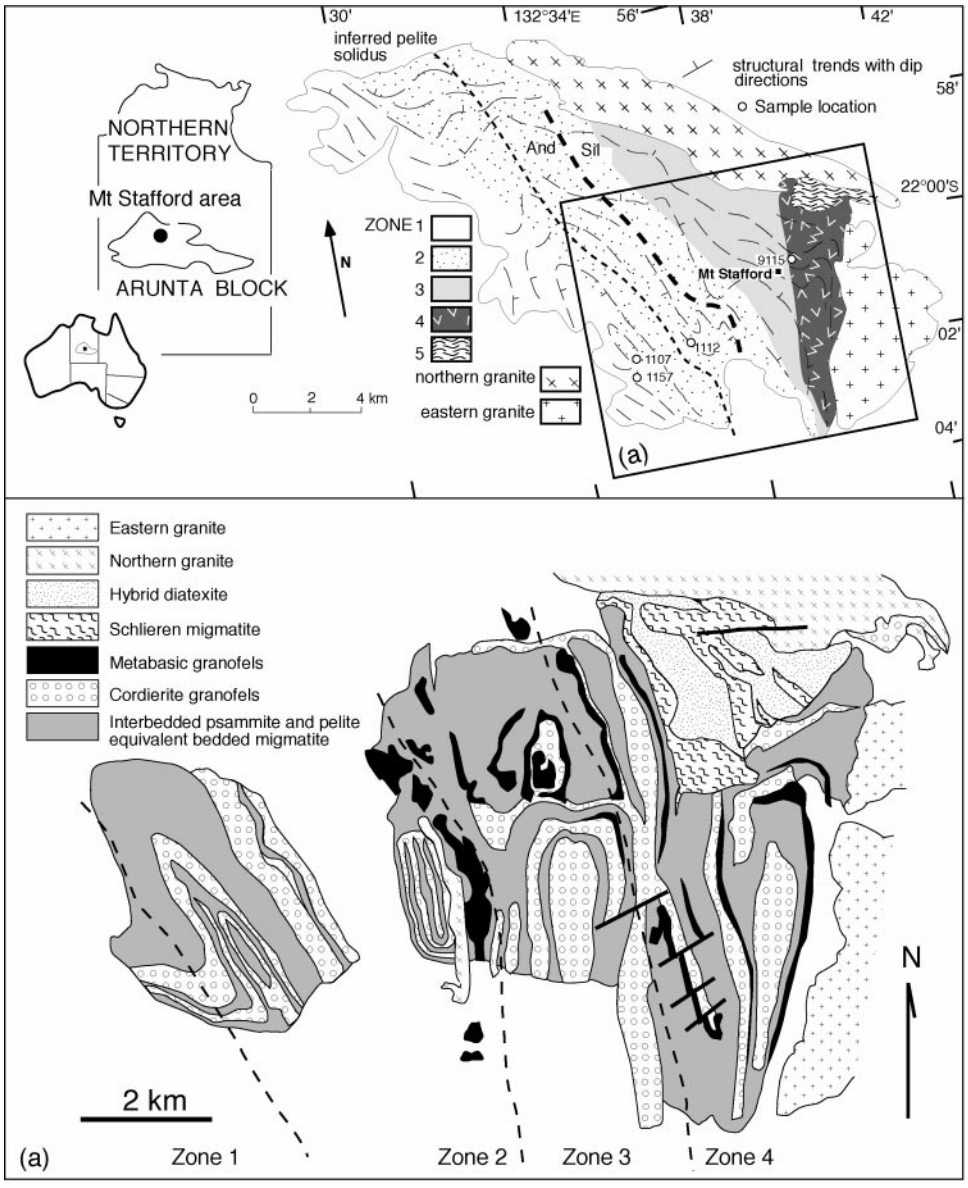

Fig. 1. Location and geological map of Mt Stafford showing the zone boundaries, general structural trends and location of samples referred to in the text. Inset (a) shows the distribution of rock types in part of the area.

Metapelite layers in Zone 3 and Zone 4 bedded migmatite commonly lack distinct leucosome, with fine (2–10 mm) leucosome-forming networks enclosing porphyroblasts. However, the partial to complete mobilization of layers with and without distinct leucosome, forming diatexite or schlieren migmatite, indicates that a considerable melt proportion must have been present (Vernon *et al.*, 1990; Greenfield *et al.*, 1996). Where Zone 3 and Zone 4 metapelite layers do not contain distinct leucosome and were not demonstrably mobilized, we infer that there was extensive interconnection of melt on, for example, a decimetre scale, but without destroying primary sedimentary features (Vernon *et al.*, 1990). In these zones, the efficiency of melt segregation was also locally highly variable, again probably as a result of heterogeneity in D_{1a} strain. In Zone 4 schlieren migmatite and diatexite, metapsammite layers behaved as more rigid blocks that were broken and rotated in a mobile, metapelitic, diatexite matrix (Greenfield *et al.*, 1996). Peak metamorphism and melting were contemporaneous with localized extension in the migmatites, evidenced by the migration of melt to boudin necks and narrow (1 cm wide) conjugate extensional shear zones. Drag folding adjacent to high-grade shear zones, which locally truncate bedding, is also inferred to have

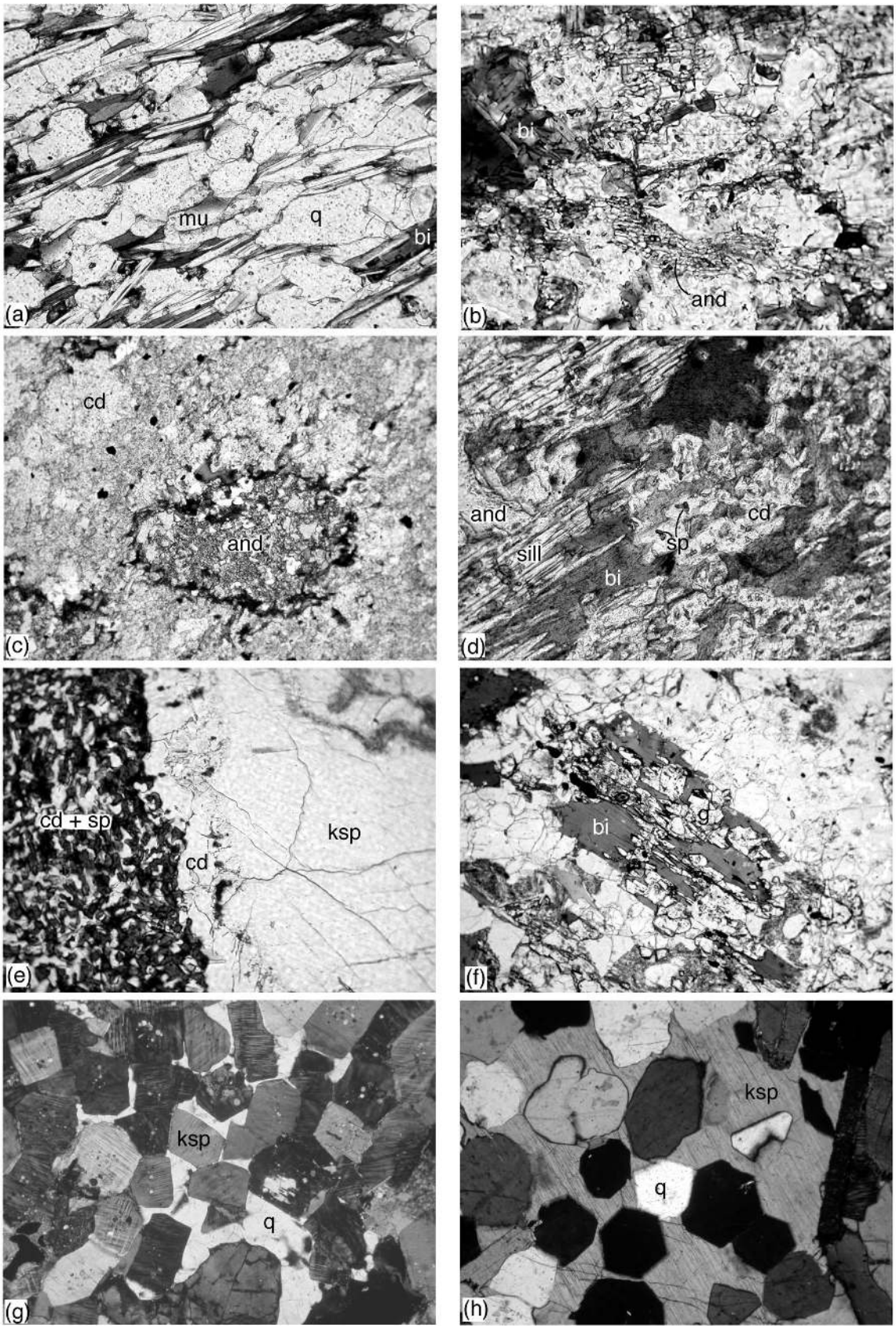

Table 1: Mineral assemblages developed in the metasedimentary rocks in each zone

Rock type	Mineral assemblages			
	Zone 1	Zone 2	Zone 3	Zone 4
Aluminous metapelite	mu–bi–q–and	cd–ksp–bi–q–and/sill	cd–ksp–q–sill	cd–ksp–q–sill
			cd–ksp–sp–bi–sill	cd–ksp–sp–sill
			cd–ksp–sp–sill	
Subaluminous metapelite	mu–bi–q	cd–ksp–bi–q–and/sill	cd–ksp–bi–q	cd–ksp–bi–q
	mu–bi–q–and		cd–ksp–bi–q–g	cd–ksp–q
			cd–ksp–sp–bi–sill	cd–ksp–sp
			cd–ksp–sp–bi	cd–ksp–bi–sp
				cd–ksp–q–g
Metapsammite	mu–bi–q	cd–ksp–bi–q–and/sill	cd–ksp–bi–q	cd–ksp–q–g–opx
			cd–ksp–bi–q–g	cd–ksp–q–g
				cd–ksp–q–opx
Cordierite granofels	mu–bi–q–cd–and	cd–bi–q–ksp	cd–bi–q–ksp	cd–q–ksp
	bi–q–cd–ksp	cd–ksp–bi–and/sill	cd–ksp–q–sill	opx–cd–q–ksp
	bi–q–cd–ksp–and	cd–ksp–bi–q–and/sill	cd–ksp–bi–sill–sp	g–cd–q–ksp
			cd–ksp–bi–q–sill	cd–ksp–q–sill
				cd–ksp–bi–sill–sp

occurred at peak conditions on the basis of shear zone–leucosome relationships. It is currently unclear what ultimately caused the localized, exceptionally low-P/high-T metamorphism.

Kilometre-scale, open to tight, NW-trending F_{1b} folds deform the migmatites and D_{1a} extensional structures. The eastern granite (Fig. 1) cuts S_{1b}, and was dated at 1818 ± 15 Ma (Collins & Williams, 1995). Although compositionally similar to, it intruded later than, the northern granite (Fig. 1). Cordierite and K-feldspar in migmatites near this body are retrogressed to muscovite–sillimanite or muscovite–andalusite assemblages. Muscovite–quartz-dominated retrograde shear zones cut all earlier fabrics.

Petrography

The Mt Stafford rocks preserve evidence for a marked lateral increase in metamorphic grade from chlorite–muscovite-bearing greenschist-facies assemblages in Zone 1 to orthopyroxene-bearing granulite-facies assemblages in Zone 4. This metamorphic transition reflects a temperature rise of several hundred degrees. In this section we concentrate on the mineral assemblage and metamorphic texture development from rocks just below the solidus to the highest-grade rocks developed in the area. As is common in many metamorphically zoned terranes, the mineral assemblage relationships used to define the metamorphic zones are derived from a variety of rocks that may

Fig. 2 (opposite). Photomicrographs showing reaction textures in metapelite from Mt Stafford. (a) Schistosity defined by aligned muscovite and biotite in a quartz-rich metapelite schist from Zone 1. Plane-polarized light, width of view is 2 mm. (b) Upper Zone 1 metapelite with a poorly developed schistosity. The rock contains andalusite, biotite, quartz and muscovite. Andalusite occurs as small equant crystals or rarely as porphyroblasts or poikiloblasts. Plane-polarized light, width of view is 2 mm. (c) Andalusite poikiloblast in cordierite granofels from the Zone 1–Zone 2 boundary. The andalusite poikiloblast contains numerous inclusions of quartz and is mantled by a discontinuous rim of fine-grained, randomly oriented biotite. The matrix of the rock is composed predominantly of fine- to medium-grained cordierite, rich in quartz inclusions and lesser amounts of included muscovite. Plane-polarized light, width of view is 2·5 mm. (d) Quartz-absent cordierite and spinel symplectites replacing biotite and aluminosilicate porphyroblast from Zone 3. Both sillimanite and andalusite are present in the porphyroblast. The symplectite here represents the incipient quartz-absent breakdown of biotite and sillimanite. Plane-polarized light, width of view is 1 mm. (e) Detail of the outer edge of a well-developed layered symplectic corona from mid Zone 3. The left-hand side of the photo is the inner (adjacent sillimanite) part of the corona and is composed of cordierite and spinel with minor ilmenite, K-feldspar and plagioclase. This symplectite is separated from a K-feldspar-rich, quartz-bearing host by a continuous corona of cordierite. Plane-polarized light, width of view is 1·5 mm. (f) Garnet overgrowth on prograde biotite from an upper Zone 3 subaluminous metapelite. The matrix contains K-feldspar, quartz and cordierite. Plane-polarized light, width of view is 3 mm. (g) Optically continuous interstitial pool of quartz enclosing prismatic K-feldspar from a Zone 4 leucosome. The K-feldspar has idioblastic crystal faces against the quartz but less well-formed boundaries against other K-feldspar grains. The K-feldspar grains commonly contain numerous quartz inclusions. Cross-polarized light, width of view is 3 mm. (h) Optically continuous K-feldspar enclosing idioblastic quartz crystals from a Zone 4 leucosome. The quartz crystals in extinction show hexagonal outlines and are viewed along the *c*-axis. Cross-polarized light, width of view is 2·2 mm.

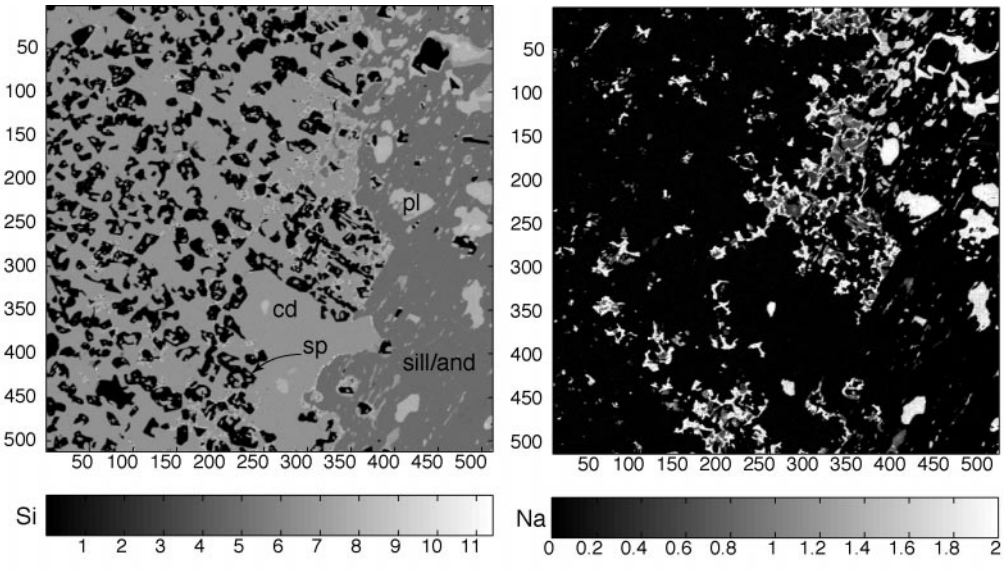

Fig. 3. X-ray maps of a spinel- and cordierite-rich symplectite enclosing an aluminosilicate porphyroblast from a mid Zone 3 aluminous metapelite. The maps show Si and Na cation distributions calculated from X-ray intensities using the method of Clarke *et al.* (2001) and calculated for 24 oxygens. Each map is approximately 1·5 mm by 1·5 mm. No quartz is present in the symplectite, which additionally contains wispy, commonly intergranular, plagioclase and K-feldspar (see Na map), particularly near the aluminosilicate porphyroblast.

represent a substantial range in bulk-rock composition. Furthermore, the heterogeneous distribution of elements within rocks may lead to compositionally distinct domains within individual samples. No single rock composition preserves the complete sequence of mineral assemblages described below, and the assemblages found in the various rock types are given in Table 1.

The rocks of Zone 1, also called the muscovite zone by Vernon *et al.* (1990), are dominantly interbedded metapsammites and metapelitic schists. These rocks are dominated by muscovite, biotite and quartz with minor chlorite, tourmaline and ilmenite (Fig. 2a). The dominant foliation in these rocks is defined by fine-grained muscovite. Andalusite, rich in quartz inclusions, occurs in some aluminous Zone 1 rocks (Fig. 2b). Cordierite is present in poorly outcropping massive metasiltstones that are inferred to be the protolith for the cordierite granofels discussed later. Towards the Zone 1–Zone 2 boundary cordierite becomes the dominant mineral in these units (Fig. 2c).

Zone 2 rocks are distinguished by the appearance of andalusite porphyroblasts and K-feldspar in metapelite and metapsammite, and commonly contain the assemblage aluminosilicate, cordierite, K-feldspar, biotite and quartz in metapelite and metapsammite. The boundary between Zones 1 and 2 is also marked by the appearance of dark spots in some metasedimentary rocks that are inferred to represent cordierite porphyroblasts that have since been pseudomorphed by symplectites of biotite, andalusite and quartz (Vernon *et al.*, 1990). Additionally, the appearance of andalusite porphyroblasts and K-feldspar in metapelite and metapsammite occurs near this zone boundary. A poorly layered cordierite-rich rock termed 'cordierite granofels' by Greenfield *et al.* (1996) becomes common in Zone 2. The cordierite granofels may contain up to 60% cordierite at this grade along with aluminosilicate, biotite, K-feldspar and quartz. Greenfield *et al.* (1996) subdivided Zone 2 into Zones 2a, 2b and 2c. The first appearance of felsic segregations marks the boundary between Zones 2a and 2b. These leucocratic segregations contain microcline with idioblastic faces within large optically continuous quartz grains, and were interpreted by Greenfield *et al.* (1996, 1998) to represent the development of partial melt from crossing the wet solidus. The boundary between Zones 2b and 2c is defined by the first appearance of sillimanite partially pseudomorphing andalusite.

The low-temperature boundary of Zone 3 is defined by a marked decrease in the mode of biotite. The appearance of spinel + cordierite-bearing symplectites that mantle aluminosilicate porphyroblasts (Figs 2d, e and 3) in Zone 3 was interpreted by Greenfield *et al.* (1996, 1998) to reflect crossing the KFMASH reaction:

$$\text{sill} + \text{bi} + \text{q} = \text{sp} + \text{cd} + \text{ksp} + \text{liq} \qquad (1)$$

(mineral abbreviations are given in Appendix A) and to represent the local complete consumption of biotite and the stabilizing of coexisting spinel + quartz. However, the X-ray map shown in Fig. 3 shows that the spinel + cordierite-bearing symplectites that

mantle aluminosilicate porphyroblasts at this grade lack quartz. Thus the development of these symplectites may reflect a different process from that implied by reaction (1). Most of these symplectic coronas have an outer layer of cordierite and an inner layer composed of a symplectic intergrowth of spinel, cordierite, K-feldspar and minor plagioclase (Figs 2e and 3). Some metapelite samples, especially those rich in aluminosilicate, lack biotite in Zone 3. Cordierite granofels commonly becomes aluminosilicate-absent in Zone 3. However, where present, the aluminosilicate porphyroblasts are also mantled by cordierite + spinel-bearing symplectites.

Garnet-bearing assemblages become common in metapsammite and less aluminous metapelite near the high-temperature end of Zone 3. Garnet commonly overgrows prograde biotite (Fig. 2f). The boundary between Zones 3 and 4 is marked by the appearance of orthopyroxene in metapsammitic rocks. Orthopyroxene may also occur in the cordierite granofels, but is absent from most samples.

In metapelitic rocks, inferred peak metamorphic assemblages involving cordierite, spinel, K-feldspar and quartz, with or without minor biotite, are most common. The assemblages sillimanite, cordierite, spinel, K-feldspar and quartz, and cordierite, spinel, garnet, K-feldspar and quartz, both with or without minor biotite are also developed. However, the distribution of minerals in many samples is patchy, and several assemblages may be developed in a single rock on a millimetre to centimetre scale.

Centimetre-scale leucocratic segregations become common in rocks above mid Zone 2, and may occur on a decimetre scale in upper Zone 3 and Zone 4. The segregations are generally K-feldspar- and quartz-rich and may additionally contain cordierite, biotite and garnet, depending on metamorphic grade. The most common types contain prismatic K-feldspar grains with crystal faces against interstitial pools of optically continuous quartz (Fig. 2g). Less commonly the K-feldspar–quartz relationships are reversed, with idioblastic quartz in optically continuous K-feldspar (Fig. 2h). Equant cordierite grains are also common in leucosomes and are also enclosed by optically continuous pools of quartz or K-feldspar. Garnet-bearing leucosomes are restricted to Zone 4, where they also preserve idioblastic faces against optically continuous quartz or K-feldspar. The idioblastic nature of the minerals in the leucosomes and the large bodies of optically continuous host minerals is consistent with their growth in the presence of melt, and in some examples their crystallization from melt (Sawyer, 1999). However, what proportion of each grain crystallized from melt, as opposed to having a sub-solidus or peritectic origin, is unclear.

MINERAL EQUILIBRIA MODELLING OF MT STAFFORD ROCKS

To relate accurately observed mineral relationships to those predicted in calculations, a model system must be chosen that describes the composition of the rocks being studied as completely as possible. Most calculations of melting processes in metapelitic compositions can be adequately modelled in the chemical system Na_2O–CaO–K_2O–FeO–MgO–Al_2O_3–SiO_2–H_2O (NCKFMASH; White *et al.*, 2001; White & Powell, 2002). However, the presence of spinel in the Mt Stafford metapelites, as well as in many other low-pressure, high-temperature terranes, requires that Fe_2O_3 and TiO_2 are also considered (White *et al.*, 2002). Thus, most of the mineral equilibria modelling of the Mt Stafford rocks is undertaken in the Na_2O–CaO–K_2O–FeO–MgO–Al_2O_3–SiO_2–H_2O–TiO_2–Fe_2O_3 (NCKFMASHTO) model system. The NCKFMASHTO system represents the combination of the NCKFMASH model system of White *et al.* (2001) and the KFMASHTO model system of White *et al.* (2002).

All the mineral equilibria calculations were undertaken using THERMOCALC 3.0 (Powell & Holland, 1988) and the Holland & Powell (1998, in the form of the September 1999 upgrade) internally consistent thermodynamic dataset. The calculations involve the minerals quartz, garnet, sillimanite, cordierite, orthopyroxene, K-feldspar, plagioclase, biotite, muscovite, spinel, magnetite, ilmenite, haematite and silicate melt. The thermodynamic models and a–X relationships for cordierite, K-feldspar, plagioclase and muscovite are those used by White *et al.* (2001). The models for biotite, spinel, magnetite and ilmenite are those given by White *et al.* (2002). The garnet model used is a combination of the a–X models of White *et al.* (2001) and White *et al.* (2002), and is presented in Appendix B.

The bulk-rock compositions used in the calculations were taken from X-ray fluorescence (XRF) analyses of metapelite and metapsammite presented by Greenfield (1997) and in Table 2. Mineral equilibria modelling of the Mt Stafford rocks was undertaken on a metapelite–metapsammite pair (samples 1107pe and 1107ps) as well as a low-Al pelite (sample 9115), a metapsammite (sample 1112) and a cordierite granofels (sample 1157c). No XRF analyses of the cordierite granofels are available, and so the bulk-rock composition used here is estimated from a combination of point-counted modal proportions and electron microprobe data for a Zone 2a sample (1157c). Because of the limited constraints on bulk-rock composition, the modelling undertaken for the cordierite granofels does not include TiO_2 and Fe_2O_3 and is undertaken in the

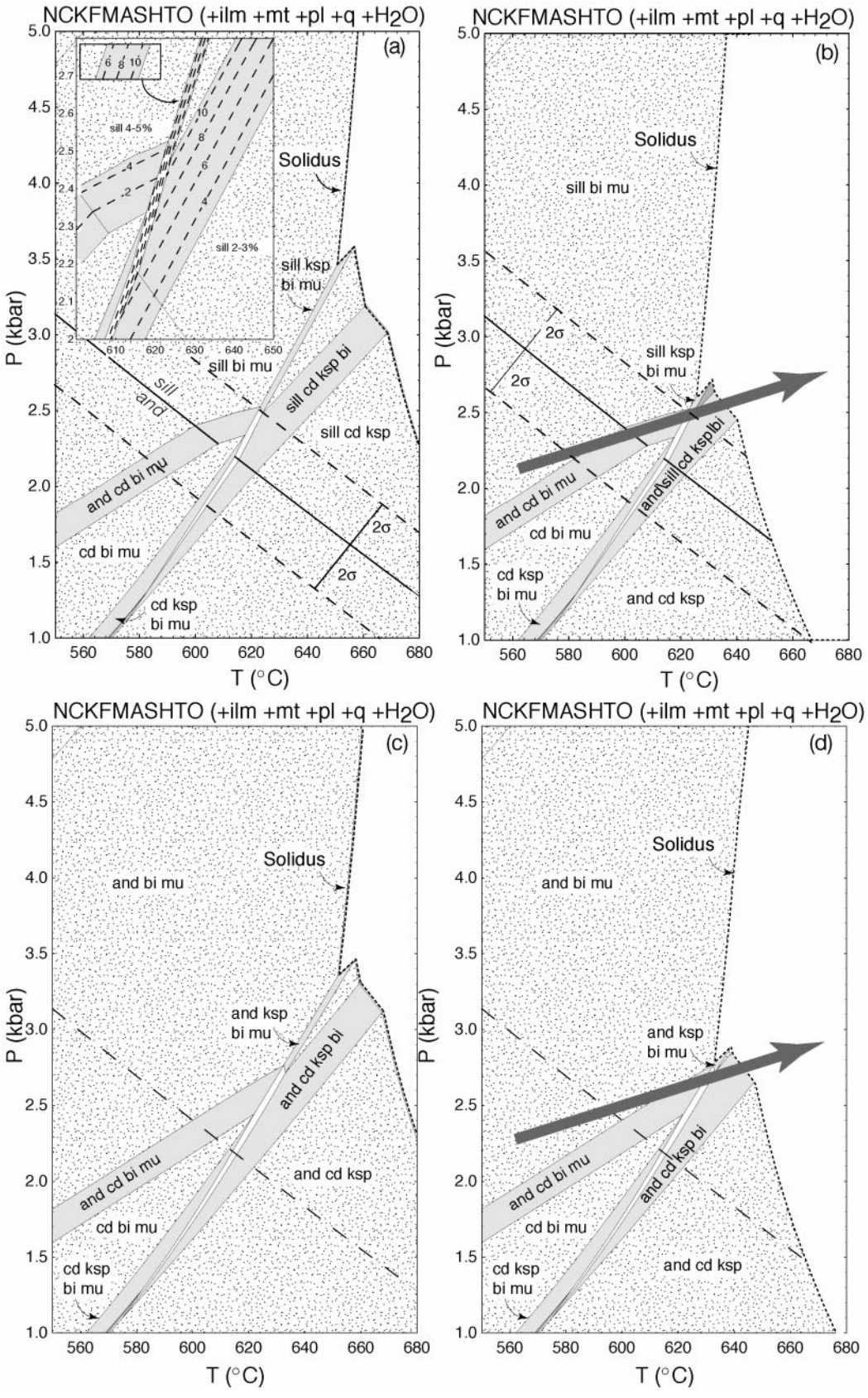

Table 2: Bulk-rock compositions used in calculations in molar oxide percent

		H_2O	SiO_2	Al_2O_3	CaO	MgO	FeO	K_2O	Na_2O	TiO_2	O
Fig. 4		12·099	67·225	9·942	0·185	2·470	4·001	2·808	0·496	0·412	0·362
Fig. 5		3·344	73·921	10·932	0·203	2·716	4·399	3·088	0·546	0·453	0·398
Fig. 6		5·009	63·600	13·418	0·378	4·427	7·015	4·041	1·017	0·706	0·391
Fig. 7		5·213	59·342	17·043	0·317	4·234	6·859	4·814	0·851	0·707	0·621
Fig. 8a	$X = 0$	3·344	73·921	10·932	0·203	0·712	6·404	3·088	0·546	0·453	0·398
	$X = 1$	3·344	73·921	10·932	0·203	6·404	0·712	3·088	0·546	0·453	0·398
Fig. 8b	$X = 0$	5·558	56·650	18·172	0·338	1·183	10·645	5·132	0·907	0·753	0·662
	$X = 1$	5·558	56·650	18·172	0·338	10·645	1·183	5·132	0·907	0·753	0·662
Fig. 9		6·006	56·354	16·089	0·453	5·308	8·411	4·845	1·219	0·847	0·468
Fig. 10a	$X = 0$	5·009	63·600	13·418	0·378	4·427	7·015	4·041	1·017	0·706	0·391
	$X = 1$	3·344	73·921	10·932	0·203	2·716	4·399	3·088	0·546	0·453	0·398
Fig. 10b	$X = 0$	6·006	56·354	16·089	0·453	5·308	8·411	4·845	1·219	0·847	0·468
	$X = 1$	5·213	59·342	17·043	0·317	4·234	6·859	4·814	0·851	0·707	0·621
Fig. 11		3·256	75·621	8·267	0·662	3·047	4·729	2·835	0·888	0·448	0·246
Fig. 12		3·526	76·313	7·909	0·168	2·554	5·468	2·611	0·642	0·406	0·403
Fig. 13		6·710	62·620	14·920	0·080	6·700	6·190	2·550	0·230	—	—
Fig. 14	$X = 0$	6·211	52·748	19·967	0·104	8·964	8·281	3·416	0·311	—	—
	$X = 1$	4·392	66·584	14·120	0·073	6·339	5·856	2·416	0·220	—	—
Fig. 15	$X = 0$	4·618	75·449	7·820	0·166	2·525	5·406	2·582	0·634	0·401	0·398
	$X = 1$	3·344	73·921	10·932	0·203	2·716	4·399	3·088	0·546	0·453	0·398

NCKFMASH model system. The main effect of ignoring TiO_2 and Fe_2O_3 is to decrease the stability range of spinel to higher temperatures and reduce the high-temperature stability limit of biotite (e.g. White *et al.*, 2002).

Metapelites

The subsolidus evolution of the metapelites primarily involves the breakdown of muscovite and the appearance of cordierite, K-feldspar and andalusite. Andalusite first appears in Zone 1 rocks, initially restricted to more aluminous compositions. The appearance of cordierite and K-feldspar, a marked increase in the mode of aluminosilicate, and the disappearance of muscovite, occur at almost the same place in the sequence, the boundary between Zones 1 and 2. Thus, it is likely that the Zone 1–Zone 2 boundary occurs close to the intersection between the subsolidus trivariant field, in which coexisting muscovite and quartz break down, and the trivariant field in which subsolidus cordierite is first produced (Fig. 4). For 1107pe (Fig. 4a) this intersection occurs at about 2·5 kbar and 625°C. This intersection moves to different P–T conditions with changing bulk-rock composition, as the development of cordierite is dependent on bulk-rock X_{Fe}.

The location of the andalusite to sillimanite transition in the Mt Stafford sequence occurs at higher grade than the inferred crossing of the wet solidus (Fig. 4). This is inconsistent with most experimental and thermodynamic data, which suggest that the wet solidus does not intersect the andalusite to sillimanite reaction. The source of this inconsistency may lie in the position of the andalusite to sillimanite reaction relative to where this transition is first observed in the sequence and/or the location of the calculated solidus. Below we discuss both these possibilities and their implications. It is possible that the andalusite to sillimanite transition

Fig. 4 (opposite). P–T pseudosections showing alternative subsolidus mineral assemblage relationships for the sample 1107pe composition. (a) P–T pseudosection for conditions of fluid in excess. Also shown are the 2σ error bars on the andalusite = sillimanite reaction. The inset shows calculated aluminosilicate mode contours for part of the diagram. (b) Semiquantitative P–T pseudosection showing the mineral relationships relative to a wet solidus depressed to lower temperatures because of the presence of boron. The position of the solidus is not calculated but is shifted to lower temperatures manually. Also shown are the 2σ error bars on the andalusite = sillimanite reaction. The grey arrow shows the position of a field gradient in P–T that is consistent with the petrographic observations assuming sillimanite replaces andalusite at the calculated reaction. (c) P–T pseudosection calculated assuming the metastable persistence of andalusite to temperatures above the calculated andalusite = sillimanite reaction. (d) Semiquantitative P–T pseudosection showing the mineral relationships relative to a wet solidus depressed to lower temperatures and the metastable persistence of andalusite. The grey arrow shows the position of a field gradient in P–T that is consistent with the petrographic observations assuming andalusite metastably persists beyond its calculated stability.

preserved at Mt Stafford does not occur at the same conditions as the calculated or experimentally derived andalusite to sillimanite reaction. The metastable persistence of aluminosilicate minerals outside their stability range is documented in a number of studies (e.g. Kerrick, 1990). The metastable growth of minerals is less commonly inferred to occur (e.g. Motoyoshi *et al.*, 1990). Andalusite may persist, along with sillimanite, in many of the Mt Stafford rocks to Zone 4 conditions. Whether or not simply the metastable persistence of andalusite or the metastable growth of andalusite needs to be invoked to explain the occurrence of andalusite at conditions outside its stability range depends on whether the mode of aluminosilicate is increasing or decreasing along each rock's P–T path. If the mode of aluminosilicate is increasing along the up-temperature part of the prograde path, it is likely that sillimanite would appear in the sequence close to the reaction andalusite = sillimanite, unless sillimanite has difficulty nucleating. However, if the mode of aluminosilicate is decreasing along the same path, only the metastable persistence of andalusite into the sillimanite field is required. Aluminosilicate mode contours are shown in Fig. 4a for the P–T region in question. Aluminosilicate modes are close to constant or decreasing until the muscovite + quartz breakdown reaction is reached and a small jump in aluminosilicate mode is predicted. Above this reaction, aluminosilicate modes decrease with rising temperatures. Thus, with the exception of the muscovite + quartz breakdown reaction, aluminosilicate modes generally decrease with rising temperature.

The substantial uncertainties on the andalusite = sillimanite reaction are shown in Fig. 4a and b. The error bars shown are the 2σ errors calculated by THERMOCALC. Furthermore, the presence of minor elements, such as ferric iron, in aluminosilicates, may shift the equilibria in P–T space. The muscovite + quartz breakdown reaction may occur in the andalusite field at pressures below about 2·5 kbar for the upper andalusite = sillimanite error limit. Below this pressure andalusite is the stable polymorph produced where the mode of aluminosilicate increases. Given the observation of metastable persistence of andalusite into the sillimanite stability field from several studies (Vernon *et al.*, 1990; Greenfield *et al.*, 1996), it is possible that sillimanite did not grow in these rocks until temperatures at which the kinetic barriers to this reaction had been overcome and/or the mode of aluminosilicate began to increase. If sillimanite is not produced at the andalusite = sillimanite reaction, mineral equilibria relationships involving aluminosilicate are the metastable andalusite-bearing ones. This will have an effect on the position and slope of aluminosilicate-bearing fields. Figure 4c shows the subsolidus mineral equilibria relationships calculated with andalusite metastably persisting.

The wet solidus in the calculations occurs at temperatures well above the calculated andalusite to sillimanite transition, even when the substantial uncertainties of this reaction are taken into account. The presence of boron and/or fluorine in fluids will lower the temperature of the solidus (Chorlton & Martin, 1978; Kerrick & Speer, 1988; London *et al.*, 1996). Greenfield *et al.* (1996, 1998) suggested the breakdown of detrital tourmaline in the metasediments as a potential source of boron. However, the overall distribution of tourmaline and the distribution of boron-bearing fluids in the terrane are unconstrained, and Greenfield (1997) suggested that melting both before and after the crossing of the andalusite to sillimanite reaction was possible in different parts of the terrane. The relationships between mineral reaction and the wet solidus, if depressed to lower temperatures by boron and/or fluorine, can be shown in a semi-quantitative pseudosection (Fig. 4b and d). However, the amount the solidus can be shifted to lower temperatures is limited by the need to have muscovite breakdown occur under subsolidus conditions. Thus the solidus at Mt Stafford cannot be shifted to lower temperatures by much more than about 25°C. Overall, the metastable persistence of andalusite and probably the depression of the solidus are required to match the observed subsolidus mineral assemblage development.

At temperatures above the solidus the rock becomes fluid-absent. Thus, further melting relies mainly on the breakdown of hydrous minerals and the supersolidus calculations involve a fixed water content for the rock. Figure 5 is a P–T pseudosection drawn for an aluminous metapelitic composition (sample 1107pe) with a fixed water content. Modal contours are shown for several minerals in relevant fields. The water content is fixed such that there is $<1\%$ modal water in the rock at the solidus, between where it is intersected by the subsolidus muscovite breakdown reaction and the subsolidus biotite and sillimanite breakdown reaction ($P \approx 3{\cdot}2$ kbar, $T \approx 640$°C).

Because of the small modal water content immediately below the solidus, little melt is produced at the solidus. With rising temperature biotite and sillimanite modes rapidly decrease as cordierite and melt contents increase, which is consistent with the observed mineral assemblage relationships at the Zone 2–Zone 3 boundary. Initially, the leucosome is concentrated in patches around the large aluminosilicate porphyroblasts in the form of millimetre- to centimetre-wide moats. Hence, this melting relationship is restricted to, or at least concentrated around, the isolated aluminosilicate porphyroblasts. Thus the leucosome distribution reflects the pre-existing textural features of the rock. The large

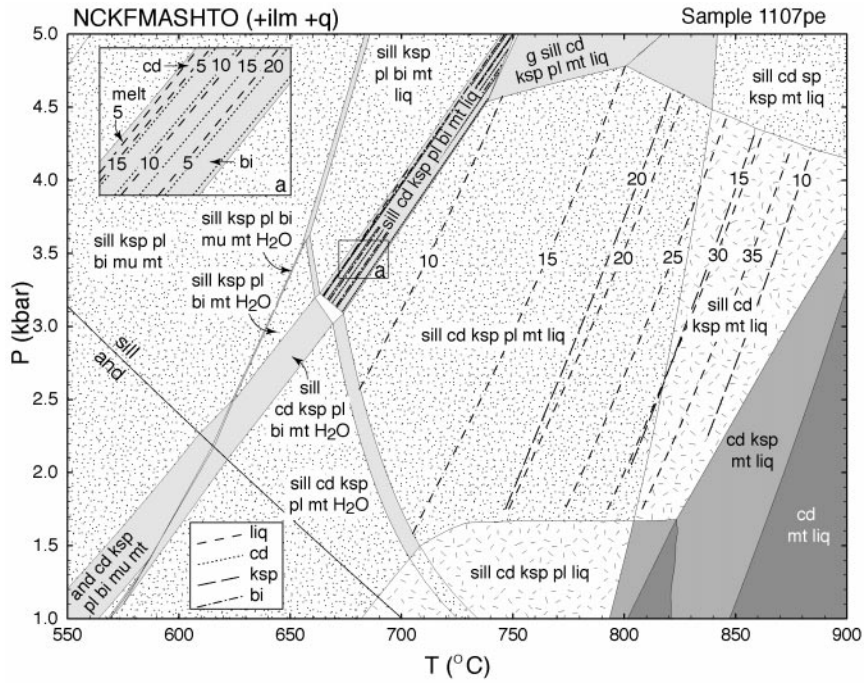

Fig. 5. Calculated P–T pseudosection for the supersolidus part of sample 1107pe (aluminous metapelite). Because of the need to fix water contents in the bulk rock at the solidus, the water-absent subsolidus fields are inappropriate for interpreting the pre-melting prograde evolution. The pseudosection also shows calculated molar mode contours in percent for several minerals and silicate melt. Insert (a) shows detail of the mode changes that occur within the area indicated by the box. The quartz-bearing aluminous metapelites have a relatively simple evolution at temperatures above the breakdown of biotite and develop an assemblage dominated by cordierite, K-feldspar and silicate melt in upper Zone 3 and Zone 4.

aluminosilicate porphyroblasts may effectively partition the bulk-rock composition into high- and low-alumina domains at this grade. In high-alumina domains, the aluminosilicate:biotite ratio was such that biotite was consumed before aluminosilicate. However, in low-alumina domains, sufficiently isolated from aluminosilicate porphyroblasts, biotite stability would persist to higher temperatures. Naturally, there would be a complete spectrum of compositions between these two end-member domains. The reaction between biotite and sillimanite is further complicated by the possibility that the rocks may locally become quartz-absent during this reaction, as quartz is also consumed.

At temperatures above the breakdown of coexisting sillimanite, biotite and quartz, little change in the mineral assemblage occurs in aluminous metapelite. An assemblage involving primarily cordierite, sillimanite, K-feldspar, quartz and melt is stable up to Zone 4. However, with rising temperature, rates of diffusion, and hence volumes of equilibria, are likely to increase. Thus, the continued reaction between previously isolated biotite and aluminosilicate would be expected. In subaluminous metapelite (9115), garnet is produced at temperatures above about 750°C for pressures close to 3·2 kbar (Fig. 6). Garnet is common in mid to upper Zone 3 subaluminous metapelite. Garnet growth primarily occurs at the expense of biotite, matching the observed garnet overgrowths on biotite (Fig. 2f). Available biotite is progressively consumed with rising temperature, resulting in a Zone 4 assemblage dominated by cordierite, K-feldspar, quartz and melt with minor garnet. Orthopyroxene-bearing assemblages are predicted for this sample at pressures below about 3·2 kbar (Fig. 6). As orthopyroxene does not occur in metapelite samples, it is likely that pressures near the Zone 3–Zone 4 boundary were above this.

The occurrence of quartz-absent symplectites of cordierite + spinel mantling aluminosilicate porphyroblasts is consistent with silica-undersaturated domains having formed during the breakdown of coexisting sillimanite, biotite and quartz, with available quartz being consumed first. The development of the quartz-absent domains can be analysed via a P–T pseudosection (Fig. 7) based on the 1107pe composition with reduced silica, such that the rock runs out of quartz during the major melting step involving the breakdown of aluminosilicate, biotite and quartz to form predominantly cordierite and melt. Thus the diagram is quartz-bearing and identical to Fig. 5 at temperatures below this field. The most notable effect of the absence of quartz is the stabilization of spinel in these rock compositions. Although coexisting spinel and quartz may be stable at these conditions, their presence

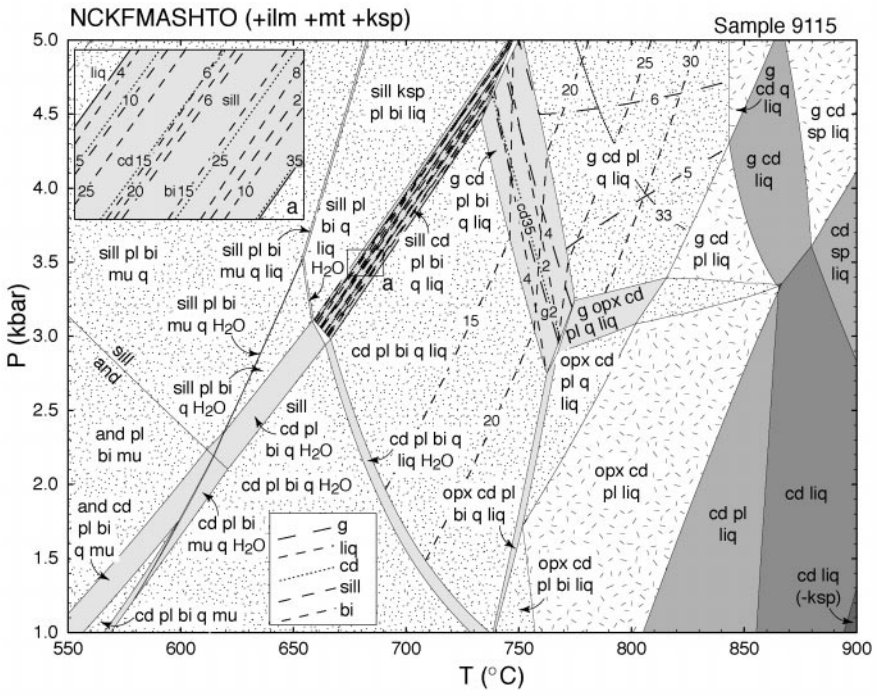

Fig. 6. Calculated P–T pseudosection for the supersolidus part of sample 9115pe (subaluminous metapelite). Because of the need to fix water contents in the bulk rock at the solidus, the water-absent subsolidus fields are inappropriate for interpreting the prograde evolution. The pseudosection also shows calculated molar mode contours in percent for several minerals and silicate melt. Insert (a) shows detail of the mode changes that occur within the area indicated by the box. The quartz-bearing subaluminous metapelites have a more complex high-grade evolution, with biotite breakdown occurring both by reaction with sillimanite [insert (a)] and during the growth of garnet.

is restricted to more Fe-rich bulk-rock compositions ($X_{Mg} < 0{\cdot}23$; Fig. 8) than reported from Mt Stafford ($X_{Mg} \approx 0{\cdot}3$–$0{\cdot}4$; Greenfield *et al.*, 1998). The presence of zinc in spinel stabilizes it in the presence of quartz to lower temperatures, and this may also have an effect on the observed metamorphic sequence compared with that predicted by the mineral equilibria modelling. Specifically, the presence of zinc will probably lower the temperature of the spinel-bearing equilibria, such that the quartz-present and quartz-absent breakdown of coexisting biotite and aluminosilicate occur within a narrower temperature range than shown in the pseudosections.

In Fig. 7 the reaction between biotite and sillimanite is two-stage, representing quartz-present and quartz-absent conditions, respectively. The quartz-present breakdown of biotite and sillimanite produces mostly cordierite, K-feldspar and melt. This reaction terminates when available quartz is consumed. Further reaction of remaining biotite and sillimanite under quartz-absent conditions is initiated some 40°C above the temperature at which the quartz-present reaction ceased. However, the temperature difference between the quartz-present and quartz-absent breakdown of biotite and sillimanite will vary depending on bulk-rock composition. The quartz-absent reaction of biotite and sillimanite produces predominantly cordierite, spinel, K-feldspar and melt, and ceases when available biotite is consumed. In contrast, sillimanite may be consumed before biotite (Fig. 9), resulting in an assemblage of predominantly cordierite, spinel, K-feldspar, biotite and melt. The presence of layered symplectic coronas consisting of an outer cordierite layer and an inner layer of symplectic cordierite and spinel is consistent with the predictions of the model (Fig. 2f). In less aluminous metapelites the symplectites of cordierite and spinel commonly lack an aluminosilicate core, consistent with sillimanite being completely consumed during the quartz-absent reaction between biotite and sillimanite.

The various mineral assemblages developed in the metapelites are essentially controlled by two main compositional variables: $X_{Al_2O_3}$ and X_{SiO_2}. $X_{Al_2O_3}$ affects mainly the presence or absence of aluminosilicate at higher grades, and X_{SiO_2} mostly affects the presence or absence of quartz or spinel in different compositional domains. In both silica-saturated and silica-undersaturated domains, the survival of aluminosilicate porphyroblasts through Zones 3 and 4 is strongly dependent on bulk-rock composition, especially $X_{Al_2O_3}$, as shown in Fig. 10. This figure shows two T–X_{bulk} pseudosections drawn for $P = 3{\cdot}3$ kbar, with X ranging from the sample 9115 composition to the sample 1107pe composition. The main compositional

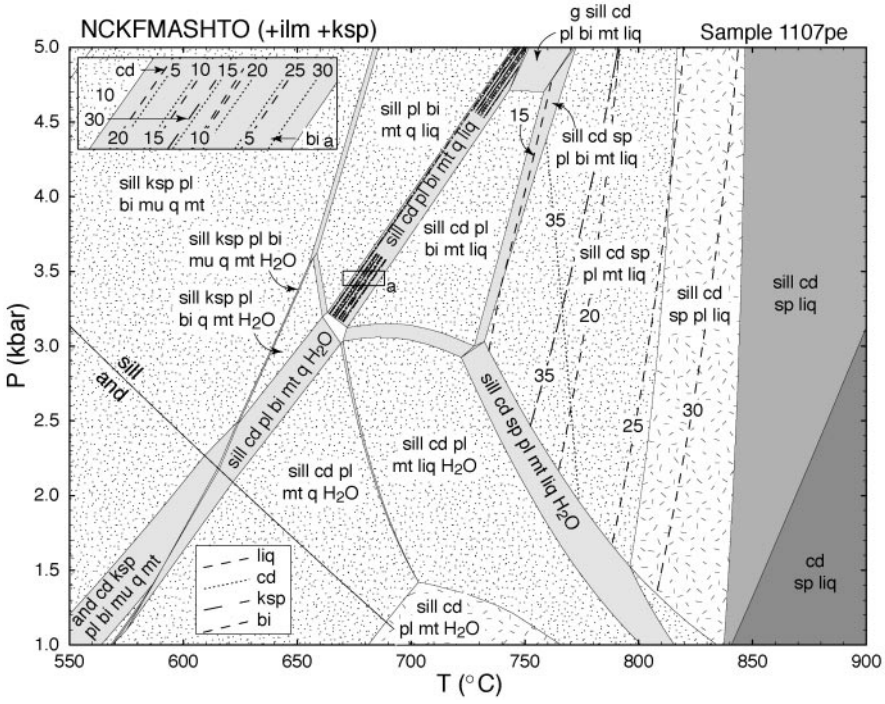

Fig. 7. Calculated P–T pseudosection for the supersolidus part of an aluminous metapelite with a bulk-rock composition appropriate to the development of quartz-absent domains during the initial breakdown of coexisting biotite, sillimanite and quartz. The bulk composition was derived by removing silica from the sample 1107pe composition used in Fig. 5. Because of the need to fix water contents in the bulk rock at the solidus, the water-absent subsolidus fields are inappropriate for interpreting the prograde evolution. The pseudosection also shows calculated molar mode contours in percent for several minerals and silicate melt. Insert (a) shows detail of the mode changes that occur within the area indicated by the box. The quartz-absent breakdown of biotite and sillimanite occurs 20–40°C above the initial quartz present breakdown.

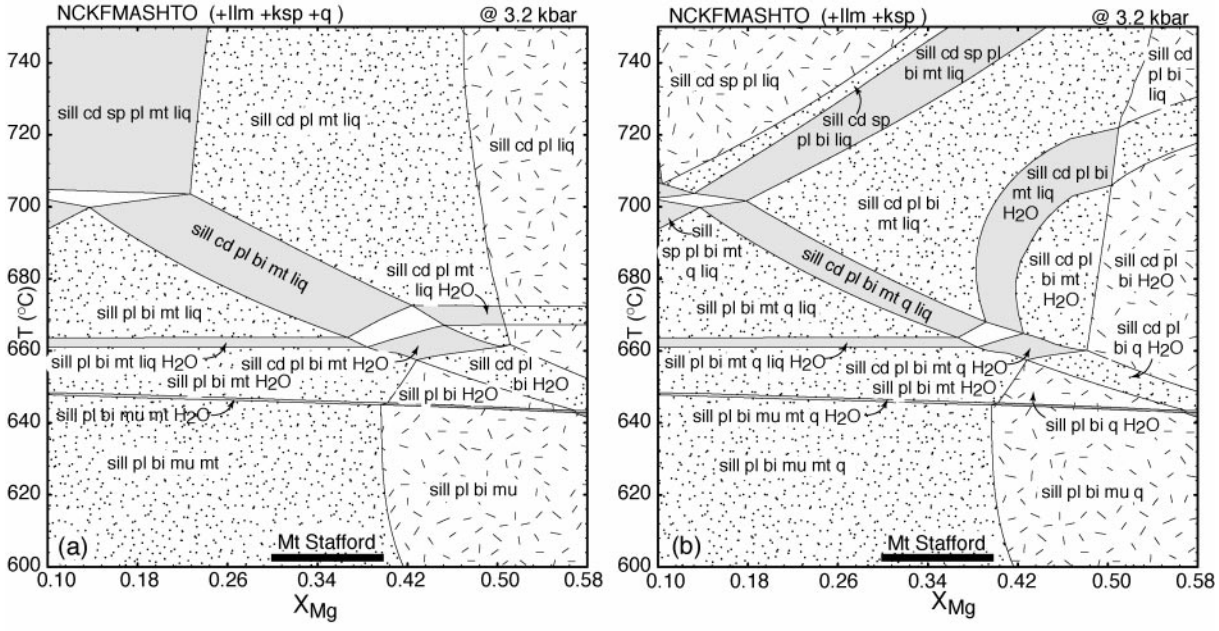

Fig. 8. Calculated T–X_{Mg} pseudosections based on the 1107pe bulk-rock composition showing the stability of spinel in both quartz-present and quartz-absent aluminous metapelite. The black bars labelled Mt Stafford show the range of X_{Mg} for the Mt Stafford metapelites. (a) T–X_{Mg} pseudosection for quartz-bearing domains. Spinel in this model requires bulk-rock $X_{Mg} < 0{\cdot}23$. (b) T–X_{Mg} pseudosection for domains that lose quartz during the quartz-bearing breakdown of biotite and sillimanite. Here, quartz-absent, spinel-bearing assemblages will be developed in bulk-rock compositions appropriate to Mt Stafford. More Fe-rich bulk compositions will develop spinel at lower temperatures than the more Mg-rich rocks.

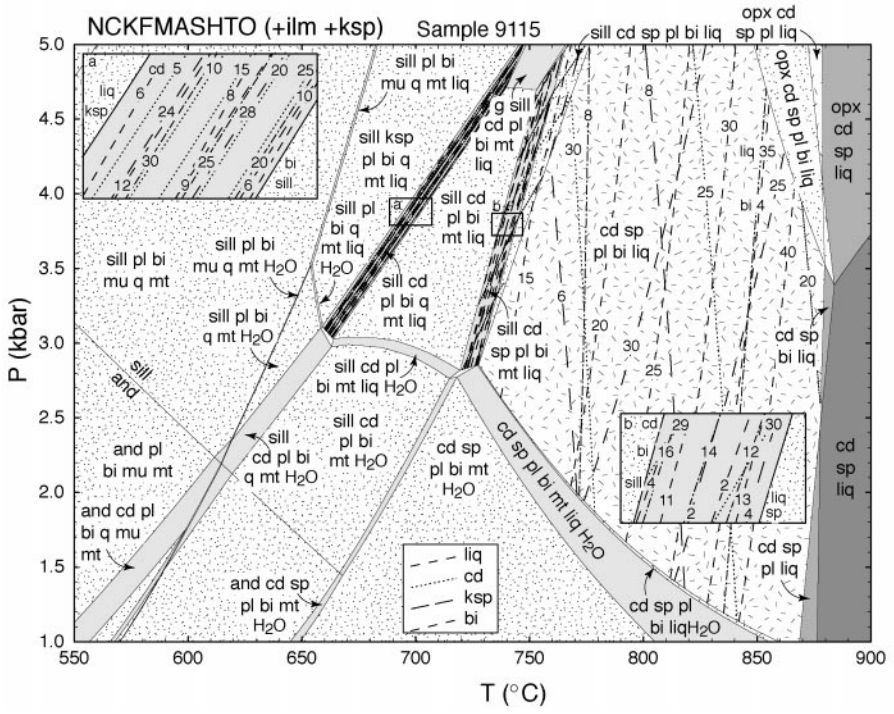

Fig. 9. Calculated P–T pseudosection for the supersolidus part of a subaluminous metapelite with a bulk-rock composition appropriate to the development of quartz-absent domains during the initial breakdown of coexisting biotite, sillimanite and quartz. The bulk composition was derived by removing silica from the sample 9115pe composition used in Fig. 6. Because of the need to fix water contents in the bulk rock at the solidus, the water-absent subsolidus fields are inappropriate for interpreting the prograde subsolidus evolution. The pseudosection also shows calculated molar mode contours in percent for several minerals and silicate melt. Inserts (a) and (b) show detail of the mode changes that occur within the areas indicated by the boxes. The quartz-absent breakdown of biotite and sillimanite occurs 20–40°C above the initial quartz-present breakdown.

variable along the X-axis is aluminium content. In Fig. 10a there is sufficient silica for the quartz-present breakdown of biotite and sillimanite to go to completion. Figure 10b shows the effect of available quartz being consumed during the initial quartz-bearing reaction between biotite and sillimanite. Thus, at temperatures below this reaction the assemblages are quartz-bearing, and above it they are quartz-absent.

The initial quartz-bearing reaction between biotite and sillimanite is terminated when local quartz, sillimanite or biotite is consumed. Above this reaction, the quartz-bearing rocks (Fig. 10a) become either biotite-absent above $X_{bulk} = 0{\cdot}56$ or sillimanite-absent below it. With rising temperature, sillimanite may be consumed in some less aluminous, biotite-absent rocks. However, in the aluminous metapelites little further mineralogical change occurs with rising temperature. The less aluminous metapelites below $X_{bulk} = 0{\cdot}56$ develop garnet predominantly at the expense of biotite at temperatures above 750°C. The quartz-absent breakdown of biotite and sillimanite to produce primarily spinel, cordierite and melt occurs over the complete range of metapelite compositions (Fig. 10b). Above this reaction the composition range is divided into sillimanite-bearing and biotite-bearing fields similar to those for the quartz-bearing rocks. A range of the predicted assemblages may occur in a single sample if compositional domains are well developed. Most Mt Stafford metapelites contain quartz-absent, spinel-bearing patches, commonly centred around aluminosilicate porphyroblasts that are hosted by a cordierite- and K-feldspar-rich rock.

Metapsammites

The metapsammites have a similar subsolidus prograde evolution to that of the metapelites (Figs 11 and 12), but their evolution departs from that of the metapelites at temperatures above the quartz-present reaction between sillimanite and biotite. In the metapsammites, sillimanite is commonly consumed via the quartz-present reaction between sillimanite and biotite to produce predominantly cordierite, melt and K-feldspar. The quartz-rich, sillimanite-poor nature of the metapsammites, compared with the metapelites, results in this reaction commonly going to completion. Thus, biotite persists to higher-temperature conditions in the metapsammites than in the aluminous

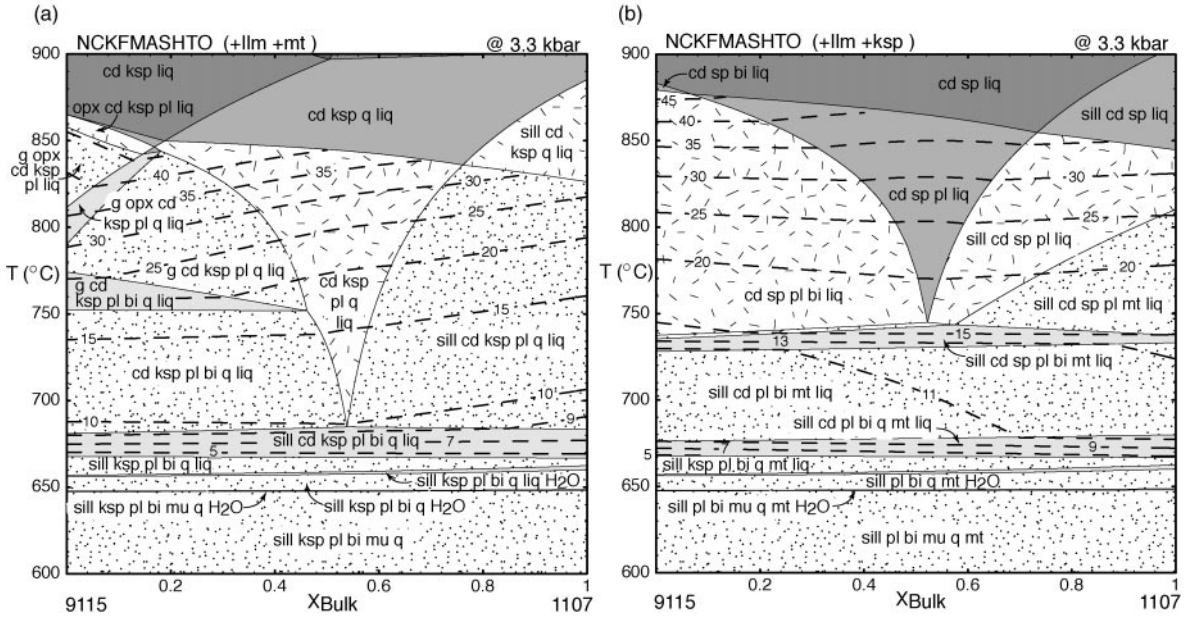

Fig. 10. Calculated T–X_{Bulk} pseudosections based on sample 9115 and sample 1107pe bulk-rock compositions. The X-axis is dominated by an increase in aluminium content from left to right. Molar melt contours are shown in both pseudosections. (a) T–X_{Bulk} pseudosection for quartz-bearing domains going from the 9115 composition at $X = 0$ to the 1107pe composition at $X = 1$. The sillimanite + biotite-absent wedge-shaped field at intermediate X values separates the subaluminous pelites (left) from the aluminous pelites (right). (b) T–X_{Bulk} pseudosection for quartz-absent domains going from the 9115 composition at $X = 0$ to the 1107pe composition at $X = 1$. The sillimanite- and biotite-absent wedge-shaped field at intermediate X values separates the subaluminous pelites (left) from the aluminous pelites (right), but starts at higher temperature than in (a).

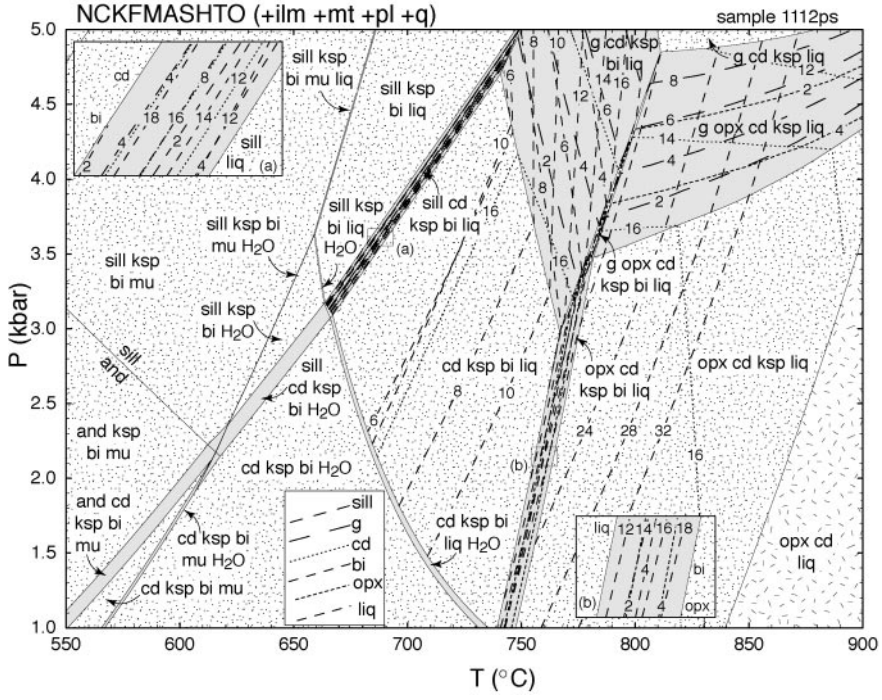

Fig. 11. Calculated P–T pseudosection for sample 1112 metapsammite. Because of the need to fix water contents in the bulk rock at the solidus, the water-absent subsolidus fields are inappropriate for interpreting the prograde evolution. The pseudosection also shows calculated molar mode contours in percent for several minerals and silicate melt. Insert (a) shows detail of the mode changes that occur during the breakdown of coexisting biotite and sillimanite within the area indicated by the box. Further biotite breakdown occurs when garnet is produced and in the narrow divariant field in which orthopyroxene is produced.

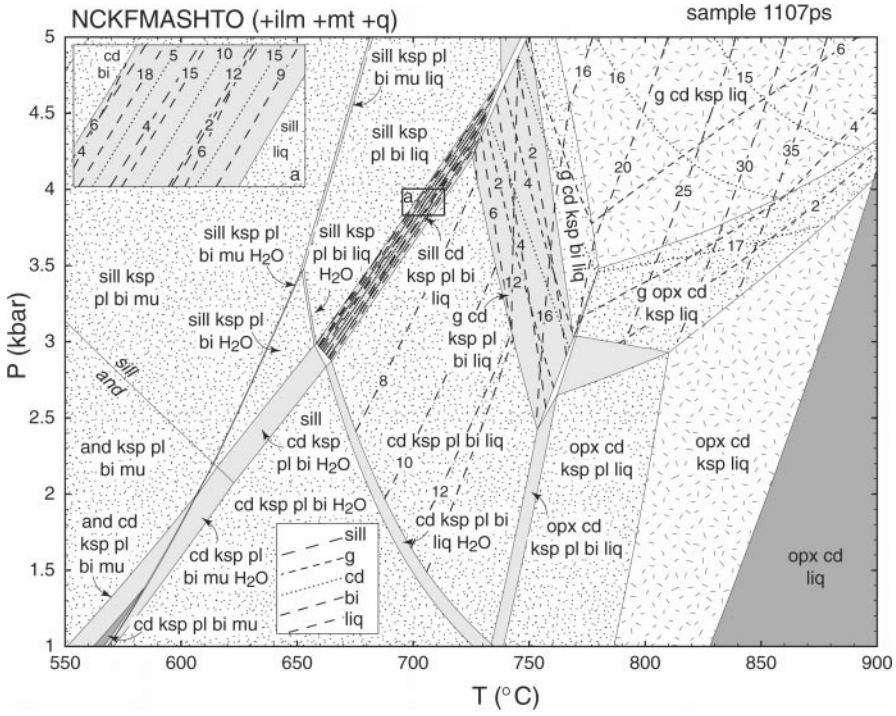

Fig. 12. Calculated P–T pseudosection for sample 1107ps metapsammite. Because of the need to fix water contents in the bulk rock at the solidus, the water-absent subsolidus fields are inappropriate for interpreting the prograde evolution. The pseudosection also shows calculated molar mode contours in percent for several minerals and silicate melt. Insert (a) shows detail of the mode changes that occur during the breakdown of coexisting biotite and sillimanite within the area indicated by the box. Further biotite breakdown occurs when garnet is produced and, at low pressures, in the narrow field in which orthopyroxene is produced.

metapelites. At temperatures above about 750°C and pressures above 3–3·5 kbar, garnet is stabilized in the assemblage, consistent with observations for upper Zone 3 rocks. Further heating leads to the development of orthopyroxene and the concurrent loss of biotite at pressures above about 3 kbar. This mineral assemblage relationship marks the boundary between Zones 3 and 4. The formation of orthopyroxene occurs over a restricted temperature range for the appropriate bulk-rock compositions (Figs 11 and 12). However, the P–T conditions for the formation of garnet are more sensitive to bulk-rock composition (Figs 11 and 12). For metapsammite 1107ps (Fig. 12), garnet forms at lower temperature than for metapsammite 1112. Further heating for the 1107 composition to peak Zone 4 temperatures would produce a mineral assemblage containing garnet, orthopyroxene and cordierite. In contrast, garnet becomes unstable soon after its formation at pressures between 3 and 3·5 kbar for metapsammite 1112 (Fig. 11). Given the very narrow temperature range over which garnet is stable at 3–3·5 kbar it is possible, if conditions at Mt Stafford fall within this range, that garnet may not have ever nucleated in such metapsammites before it became unstable again.

Spinel is rarely found in metapsammite, but where present, is restricted to quartz-absent symplectites of cordierite, spinel and commonly minor biotite. These symplectites were most probably formed in the same way as identical symplectites in the metapelites.

Cordierite granofels

Despite the abundance of cordierite granofels in the Mt Stafford area, little detailed metamorphic analysis has been previously undertaken on it, as it lacks the complex migmatitic structure of the metapelitic rocks. The estimated bulk-rock composition of the cordierite granofels is substantially more magnesian and less aluminous, in terms of the components Al_2O_3–FeO–MgO, and less potassic than the metapelites. Samples of the cordierite granofels show a wide range in quartz content from quartz-absent to moderately quartz-rich. Greenfield (1997) measured quartz abundances from 3% to 60% for samples of the cordierite granofels by point counting.

The subsolidus metamorphic evolution of the cordierite granofels differs substantially from that of the metapelite and metapsammite. Rare cordierite-rich rocks from upper Zone 1–lower Zone 2 commonly

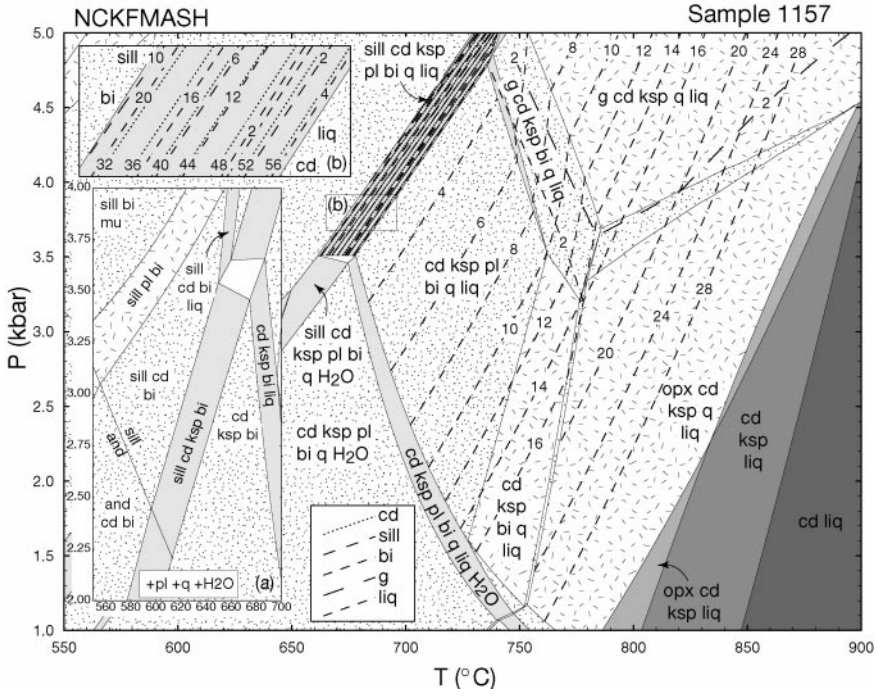

Fig. 13. Calculated P–T pseudosection for sample 1157c cordierite granofels. Because of the need to fix water contents in the bulk rock at the solidus, the water-absent subsolidus fields are inappropriate for interpreting the prograde evolution. Insert (a) shows the water-saturated prograde evolution. The pseudosection also shows calculated molar mode contours in percent for several minerals and silicate melt. Insert (b) shows detail of the mode changes that occur during the breakdown of coexisting biotite and sillimanite within the area indicated by the box. The subsolidus relationships and the position of the solidus differ markedly from those of the metapelite and metapsammite, and above the solidus the mineral assemblages are dominated by cordierite and K-feldspar.

lack muscovite, and have a peak metamorphic assemblage of cordierite, biotite, andalusite and quartz. The presence of cordierite in these rocks reflects their more magnesian composition, and is consistent with the calculations illustrated in Fig. 13a, a P–T pseudosection based on the composition of 1157c. In this pseudosection, muscovite breaks down at much lower temperatures than for the metapelites and metapsammites, and cordierite appears at temperatures approximately 100°C lower than for the metapelites. In the lower parts of Zone 2, K-feldspar becomes common in the cordierite granofels and the rocks typically have the assemblage cordierite, K-feldspar, biotite, andalusite and quartz. Cordierite dominates this assemblage and may form up to 50% of the rock at this grade. For the model composition, aluminosilicate becomes unstable about 30°C above the development of K-feldspar. However, variations in aluminium and silica contents strongly affect the stability range of aluminosilicate, and in more aluminous samples aluminosilicate would be expected to persist to higher grades.

The solidus for the modelled cordierite granofels is at slightly higher temperatures than for the metapelite composition (Fig. 13a), and the assemblage cordierite, K-feldspar, biotite, quartz, and melt, inferred for rocks from upper Zone 2 to Zone 4, is developed (Fig. 13). For the model composition, orthopyroxene becomes stable and biotite unstable at temperatures above about 780°C. Orthopyroxene is rare in the cordierite granofels, but where present is restricted to Zone 4. The presence or absence of orthopyroxene at this grade is highly dependent on bulk-rock composition, especially subtle variations in aluminium content. Furthermore, the absence of TiO_2 and Fe_2O_3 from the model calculations may affect the location of orthopyroxene-bearing fields.

Some lower-grade cordierite granofels samples lack quartz or have all the quartz occurring as inclusions in other minerals, especially cordierite. In many higher-grade samples, quartz is restricted to discrete leucosomes, where it occurs as large optically continuous grains that enclose idioblastic K-feldspar and cordierite, and is inferred to be a product of melt crystallization. Thus, it is likely that many of these rocks became quartz-absent during prograde metamorphism. The effects of the cordierite granofels becoming quartz-absent during prograde metamorphism can be addressed using a T–X_{SiO_2} pseudosection (Fig. 14), based on the bulk-rock composition used in Fig. 14. Quartz-present parts of this figure show the same

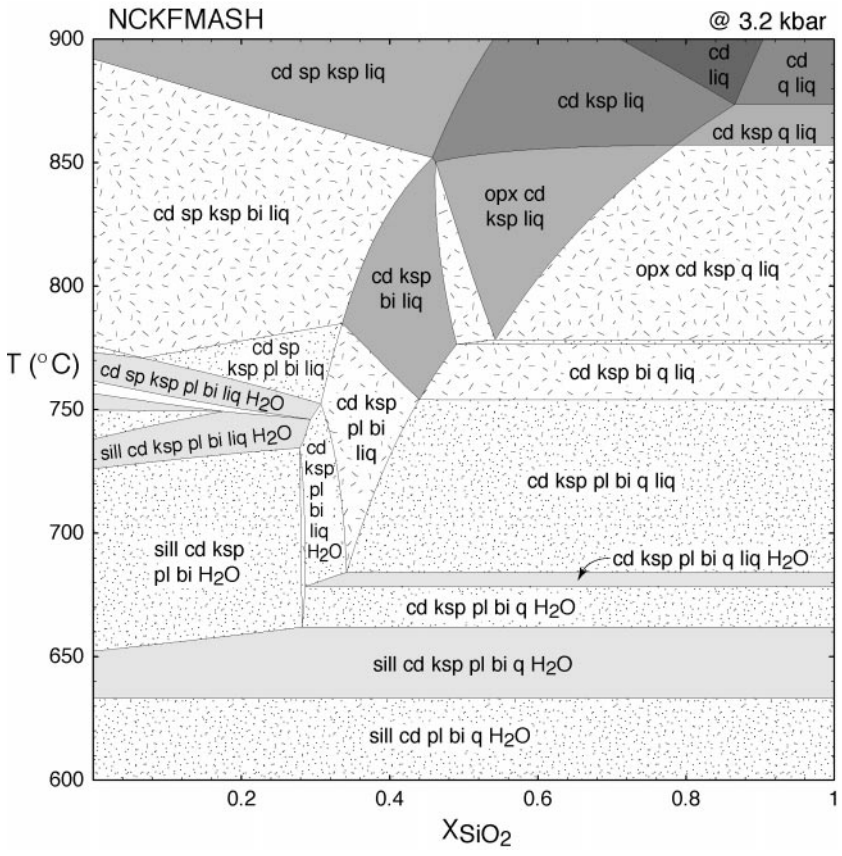

Fig. 14. Calculated T–X_{SiO_2} pseudosection of sample 1157c composition. The different mineral assemblage evolution of silica-rich and silica-poor cordierite granofels as well as different compositional domains within cordierite granofels samples can be seen for different T–X_{SiO_2} values.

history as that shown in Fig. 13. The boundary between quartz-absent and quartz-present mineral assemblages traverses the diagram from about 650°C at $X = 0$ to about 900°C at $X = 0{\cdot}9$. At very low silica contents quartz disappears at temperatures below the solidus, and sillimanite persists to higher temperatures than for the quartz-bearing rocks. The loss of quartz before melting also raises the solidus temperatures by close to 40°C. However, this is likely to have happened in only the lowest silica rocks. Further heating of low-silica rocks results in the appearance of spinel, which occurs in some samples of the cordierite granofels. Thus the spinel-present fields represent a lower limit for SiO_2 contents for these rocks. The spinel-bearing and quartz-bearing parts of Fig. 14 are separated by a series of spinel- and quartz-absent fields. Biotite persists to higher temperatures in this area, consistent with the observation of substantial inferred prograde biotite in many samples. Rock compositions in the range $X = 0{\cdot}4$–$0{\cdot}6$ lose quartz with rising temperature and melting. It is likely that the rocks that contain quartz, crystallized from melt only, are in this range.

The restriction of quartz grains to inclusions in cordierite at low grades is consistent with silica contents below $X = 0{\cdot}3$ in Fig. 14 for silica-poor examples. However, cordierite at higher grades is commonly poor in quartz inclusions. Thus, the quartz trapped at lower grades probably becomes available for reaction at higher temperatures as the rock recrystallizes. For example, a rock with an overall silica content of $X = 0{\cdot}4$ may track to the left in Fig. 14, quartz is effectively removed from the rock as quartz inclusions (e.g. to $X = 0{\cdot}2$), then the rock may track back to the right as it recrystallizes and the inclusions are destroyed.

P–T conditions of metamorphism

Within the quantitative pseudosection framework, it is possible to place more precise constraints on the P–T conditions of metamorphism and the metamorphic field gradient preserved at Mt Stafford. On the basis of thermobarometry, Greenfield *et al.* (1996, 1998) inferred the metamorphic sequence at Mt Stafford to reflect an approximately 300°C temperature difference

between the low-grade ($T \approx 500°C$) and high-grade ($T \approx 810°C$) ends. This temperature gradient is the dominant metamorphic feature in the area. In addition, thermobarometry by Greenfield *et al.* (1996) and Greenfield (1997) is consistent with a pressure increase from Zone 2 ($P \approx 2{\cdot}7$ kbar) to Zone 4 ($P \approx 4$ kbar). No assemblages suitable for P estimates were found in Zone 1. Moreover, pressure estimates across the zones all lie within 2σ uncertainties of each other, so that from thermobarometry the pressure gradient cannot be proven. The first major mineral assemblage changes occur at the Zone 1–Zone 2 boundary and provide a constraint on P–T conditions. From Fig. 4, conditions of about $P = 2{\cdot}3$–$2{\cdot}8$ kbar at $T = 620°C$ are inferred. These estimates agree well with those of Greenfield *et al.* (1996, 1998) and Greenfield (1997), namely $T = 600°C$, $P = 2{\cdot}7$ kbar.

The lower Zone 3 boundary involving a drop in biotite content in the rocks is poorly defined in the field as it does not involve the development of a new assemblage. This boundary was placed by Greenfield *et al.* (1996, 1998) at about $T = 700°C$. In the calculated pseudosections this reaction at $T = 700°C$ occurs at $P = 3{\cdot}7$–4 kbar. If the temperature estimates of Greenfield *et al.* (1996, 1998) are correct, the calculated pressure result would imply an abrupt jump in P between Zone 2 and Zone 3, for which there is no evidence. Pressures of $2{\cdot}8$–$3{\cdot}3$ kbar would be more consistent with the observations and would give temperatures of between 650°C and 680°C for the lower boundary of Zone 3. The development of garnet-bearing assemblages in upper Zone 3 metapsammites and subaluminous metapelites is consistent with $T > 740°C$ and $P > 3$ kbar (Figs 6, 11 and 12). The boundary between Zone 3 and Zone 4, defined by the appearance of orthopyroxene, is well constrained by the pseudosections at $T = 775$–$785°C$ at $P = 3{\cdot}3$–4 kbar (Figs 11 and 12). As orthopyroxene is absent from all metapelite samples, a minimum pressure estimate of $3{\cdot}3$–$3{\cdot}4$ kbar can be inferred from Fig. 6.

DISCUSSION

Previous studies of the prograde reaction sequence at Mt Stafford interpreted the textural and mineral assemblage evolution of the area to reflect the crossing of a series of univariant equilibria, in KFMASH, with rising temperature (e.g. Vernon *et al.*, 1990; Greenfield *et al.*, 1998). Although such an interpretation matches the general sequence of mineral assemblage changes, it does not include variations in rock chemistry or account for the development of distinct compositional domains within rocks. Furthermore, the petrogenetic grid used is based on assumptions, such as quartz in excess, that are not always justifiable in light of the petrological observations presented here. The quantitative pseudosection approach employed here allows a more detailed interpretation of changing mineral parageneses via multivariant equilibria, as well as providing greater constraints on the P–T conditions of metamorphism. Many features of the Mt Stafford rocks can be adequately interpreted only in terms of multivariant equilibria and varying bulk-rock compositions.

Cordierite is developed in some upper Zone 1 rocks, which are the protoliths of cordierite granofels. Furthermore, muscovite may become absent in these rocks within Zone 1. The Zone 1–Zone 2 boundary is marked by the disappearance of muscovite and the appearance of K-feldspar in metapelites and metapsammites. This boundary is broadly coincident with the appearance of cordierite in these rock types, and must involve the consumption of biotite and aluminosilicate. However, the extent to which this breakdown occurs is limited, as coexisting biotite and sillimanite persist to higher grades. The P–T conditions for cordierite production are highly dependent on bulk-rock composition. Thus, different rocks will produce cordierite at different stages in their evolution. Furthermore, compositional heterogeneities within samples on a centimetre scale appear to have resulted in slightly different mineral assemblage development histories in different parts of a given rock. The subdivision of Zone 2 by Greenfield *et al.* (1996, 1998) into three sub-zones is difficult to justify, given the complexities of deformation postdating the melting and the importance of rock composition on the mineral equilibria relationships. Although the mineral assemblage changes used to define the Zone 2 sub-boundaries certainly occur within Zone 2, their spatial relationship in the sequence is less clear. The andalusite–sillimanite transition used to define the Zone 2b–Zone 2c boundary is unlikely to represent the conditions of the equilibrium andalusite = sillimanite reaction. Instead, andalusite metastably persists to higher temperatures. Thus, the spatial relationship between the equilibrium andalusite = sillimanite reaction and the wet solidus is unclear even if the first appearance of sillimanite in the rocks is at supersolidus conditions.

The Zone 2–Zone 3 boundary was defined by Greenfield *et al.* (1996, 1998) as a marked decrease in the mode of biotite concurrent with an increase in the proportion of leucosome. This boundary reflects the supersolidus multivariant breakdown of biotite and sillimanite to form cordierite, K-feldspar and liquid in quartz-bearing domains and cordierite, spinel, K-feldspar and liquid in quartz-absent domains. This change in mineral assemblage is smeared out, both in terms of P–T conditions and in the field, and cannot be considered an isograd. The boundary between Zones 3

and 4, defined by the appearance of orthopyroxene in metapsammite, reflects a reaction between garnet and biotite, but is again restricted to a relatively small range of bulk compositions.

The subsolidus textural development of the metapelites established compositional domains because of the growth of porphyroblastic andalusite. The concentration of Al_2O_3 in these porphyroblasts ensured that the key melting reaction involving the breakdown of coexisting biotite, aluminosilicate and quartz was located around the porphyroblasts. This spatial control on the reaction led to the localized consumption of all quartz and the development of silica-undersaturated domains. These undersaturated domains then developed spinel-bearing assemblages. This interpretation differs markedly from that of Vernon *et al*. (1990) and Greenfield *et al*. (1996), who interpreted the spinel-bearing parts of the metapelites to represent preserved relics of earlier spinel-bearing assemblages. Vernon *et al*. (1990) and Greenfield *et al*. (1996) interpreted the spinel as reflecting the quartz-present reaction (1) above, followed by the subsequent consumption of spinel via a reaction between spinel and biotite to form garnet and cordierite. Although both the reactions inferred by Vernon *et al*. (1990) and Greenfield *et al*. (1998) do occur in one form or other in calculated KFMASH (White *et al*., 2001) and KFMASHTO (White *et al*., 2002) grids, they are restricted to bulk-rock compositions much richer in Fe than those found at Mt Stafford.

A further complexity involving the breakdown of biotite and sillimanite stems from changes in volumes of equilibration consequent to rising temperature conditions. In particular, the volume of rock surrounding aluminosilicate porphyroblasts that can chemically communicate with the porphyroblasts may have been relatively small at Zone 2 and lower Zone 3 conditions. If so, the prograde reaction between sillimanite and biotite would have been arrested once one of the local reactants had been consumed. However, as temperatures rose, progressively larger volumes of rock would have achieved chemical communication with the aluminosilicate porphyroblasts, allowing further reaction. Thus, the composition of small regions centred around the aluminosilicates would have changed from higher Al_2O_3 to lower Al_2O_3 with rising temperature and increasing volumes of equilibration. Such a process would have the effect of extending the presence of both aluminosilicate and biotite in a given rock to higher temperatures than those predicted by the models. However, mineral assemblages closely match those predicted for upper Zone 3 and Zone 4 rocks, consistent with diffusion being sufficiently fast and volumes of equilibration being sufficiently large that the sample size used for the XRF analysis was close to the volumes of equilibration. An important implication of the spatial focusing of the biotite breakdown reactions around aluminosilicate porphyroblasts, especially in the metapelites, is that melt production was also focused. This is most evident in upper Zone 2 and lower Zone 3 rocks, where leucosome is restricted to pools around the porphyroblasts. Thus, at these grades, neosome (in this context leucosome + peritectic or restitic minerals in biotite-depleted areas near the porphyroblasts) probably represents the volume of equilibration. Biotite-rich areas would represent paleosome. At higher grades, this relationship broke down as volumes of equilibration increased, and the rock as a whole became neosome with leucosome and peritectic or restitic minerals occurring throughout the rock on a millimetre scale.

The melt production history at Mt Stafford is controlled by a series of biotite breakdown, melt-producing reactions. All these reactions are trivariant or quadrivariant in NCKFMASHTO. Therefore different rocks experience each reaction at slightly different P–T conditions, and each occurs over a P–T region. The multivariant biotite breakdown reactions, in a simplified form, from lowest to highest grade are

$$\text{bi} + \text{sill} + \text{q} = \text{cd} + \text{ksp} + \text{liq} \quad (2)$$

$$\text{bi} + \text{sill} = \text{cd} + \text{sp} + \text{ksp} + \text{liq} \quad (3)$$

$$\text{bi} + \text{q} + \text{cd} = \text{g} + \text{ksp} + \text{liq} \quad (4)$$

$$\text{bi} + \text{g} + \text{q} = \text{opx} + \text{cd} + \text{ksp} + \text{liq}. \quad (5)$$

Although some of these reactions would involve crossing tie-lines in a classic AFM projection [e.g. reaction (5)], others, such as reaction (4), do not. For example, reaction (4) represents the garnet–cordierite–biotite tie triangle tracking past the bulk-rock composition, such that the assemblage biotite–cordierite becomes the assemblage garnet–cordierite via the assemblage garnet–cordierite–biotite.

No single rock composition will undergo all these reactions. However, some less aluminous metapelites may experience the first three if both quartz-absent and quartz-present domains are developed, and the last reaction is restricted to metapsammites. Thus a wide array of biotite breakdown melting relationships are developed in these rocks. This is consistent with the wide range of inferred temperatures at which prograde biotite disappears, and the different amounts of leucosome observed in different rocks. For example, prograde biotite is rarely present in aluminous metapelite in rocks above mid-Zone 3, whereas it is still present in less aluminous metapelite and metapsammite at the boundary between Zones 3 and 4. The complex and

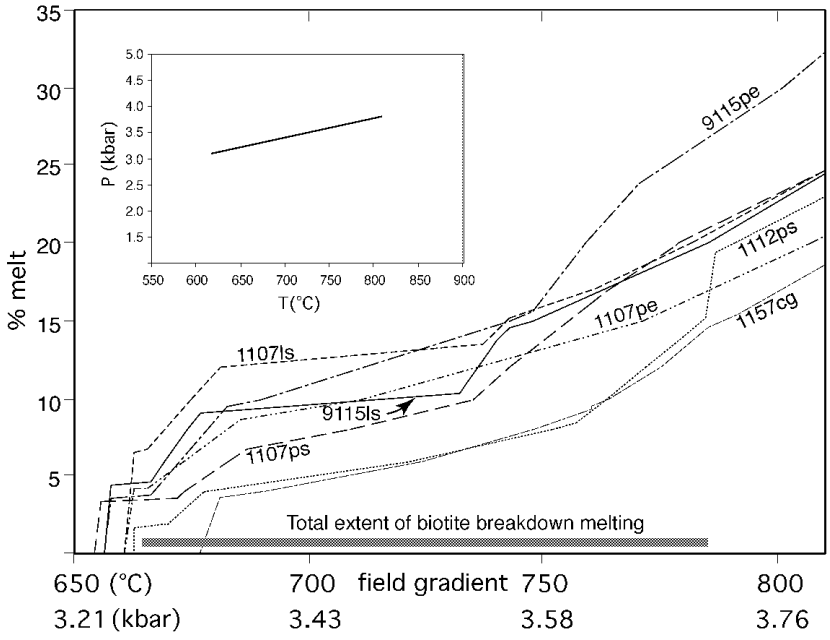

Fig. 15. Plot of melt production as a function of P–T conditions along the linear P–T vector shown in the inset for the main bulk-rock compositions discussed in the text.

staggered biotite breakdown relationships result in equally complex melting relationships. Biotite breakdown over a wide P–T range means that melt production is also smeared out over a wide P–T range. In general, the more aluminous rocks produce more melt earlier. However, biotite becomes unstable in all bulk rocks in Zone 4 and here total melt production is controlled by the total subsolidus biotite content of the rock and the amount of water tied up in cordierite at peak metamorphic conditions.

The melt production history of metasedimentary rocks at Mt Stafford can also be assessed using calculated pseudosections and compared with melt volume estimates of Greenfield *et al.* (1996) and Greenfield (1997). They established, on geochemical grounds, that the majority of the Mt Stafford metapelites lost little to none of their melt on a decimetre scale. However, the rocks show convincing evidence that melt segregation on a centimetre scale was widespread. Localized pooling of melt in extensional conjugate shears and boudin necks did occur and hence segregation on a decimetre scale. However, these are restricted, and on the basis of the geochemical studies of Greenfield *et al.* (1996), did not act as conduits for melt loss from the system on a large scale.

As with most rocks, the predicted amount of melt produced by crossing the wet solidus is small (less than 5 mol %). The main melt-producing equilibrium in the three main rock types is the quartz-present reaction between biotite and sillimanite across which 5–10% melt is produced, depending on rock composition and the availability of quartz. Further melt increases occur across the quartz-absent breakdown of biotite and sillimanite, if applicable, and during the growth of garnet at the expense of biotite in lower-Al metapelites. At temperatures above the stability of biotite in any given rock composition, melt proportions steadily increase up-temperature as the melt becomes progressively drier. A comparison of melt production as a function of temperature in the samples studied is shown in Fig. 15. In this figure, the steeper parts of each melt production curve represent the various biotite-consuming reactions. The most melt productive rocks are the subaluminous metapelites (e.g. sample 9115), which have the highest overall biotite contents. The aluminous metapelites and the metapsammites have similar peak melt productivities, but differ in their melt production curves. The metapelites produce more melt at lower temperatures, but the metapsammites undergo an additional melting step close to peak metamorphic conditions. The cordierite granofels (sample 1157) has the lowest melt production (Fig. 15), consistent with field observations of less leucosome in most outcrops. This lower melt production mostly stems from the tying up of H_2O in the abundant cordierite in these rocks, reducing available H_2O for melt production.

Molar melt contents in the upper part of Zone 3 are inferred from the modelling to be about 15–25% and

close to 30% in Zone 4, and some of these rocks form diatexites. Melt estimates by Greenfield (1997) are close to this amount. However, the estimates by Greenfield (1997) are uncertain, owing to the difficulty in distinguishing peritectic minerals from those that have crystallized from melt. The predicted amounts of melt should be adequate to allow a rock to cross a rheological critical melt percentage (25–30%, Arzi, 1978) or a broader transitional state between solid and magmatic rheologies (20–60% melt) as proposed by Renner *et al.* (2000) and become a diatexite. Importantly, most of the rocks in Zone 4 did not form diatexites, implying that in certain circumstances melt accumulation in rocks can reach as high as 30 mol % without major disruption to pre-melting structures such as bedding. However, the amount of melt required to allow a rock to transgress from a solid to a magmatic rheology will probably be dependent on the distribution of melt within the rock and the intensity of syn-metamorphic deformation, and could vary substantially from the above estimates (Brown, 1994; Brown *et al.*, 1995; Vigneresse *et al.*, 1996). The diatexites are not restricted to particular metasedimentary layers, such as subaluminous metapelite, but are most common in the bedded migmatite and rare in the cordierite granofels. The distribution of diatexite within Zones 3 and 4 may not simply reflect the distribution of the most fertile rocks, but may be strongly influenced by deformation as some of these diatexites form linear zones that cut different rock types. However, the intensity and timing of this deformation had to be such that deformation-induced melt loss on a metre to kilometre scale did not take place. The inferred low-strain deformation was insufficient to promote effective melt segregation and melt loss from the rocks. However, strain partitioning late in the metamorphic evolution was probably important in driving melt-rich rocks from metatexites to diatexites in localized zones.

The results provided by the mineral equilibria modelling are consistent with a pressure increase accompanying the temperature rise from Zone 1 to Zone 4. Thus the field gradient across the area is positively sloped in P–T. If the heat source for the metamorphism is localized, such as an igneous intrusion, then a non-linear temperature gradient would result. Although the absolute thermal source for the Mt Stafford metamorphism is not positively identified, previous workers in the area (Vernon *et al.*, 1990; Greenfield *et al.*, 1996, 1998), inferred a localized but largely hidden intrusive source for the heat. Furthermore, the intrusion of the northern granite body into partially molten migmatites in Zone 5 indicates that magmatism occurred in the area during peak metamorphism. Although the outcropping area of the northern granite is too small to be responsible for the metamorphism at Mt Stafford, it may extend under the sequence or have extended over it. Alternatively, the granite itself may be a product of another larger thermal anomaly that underlies Mt Stafford.

ACKNOWLEDGEMENTS

The research was funded by an Australian Research Council (ARC) Discovery Grant to R.P., R.W.W. and G.L.C. (DP0209461), and a University of Melbourne Small Grant to R.P. Ed Sawyer and Ron Vernon are thanked for constructive reviews.

REFERENCES

Arzi, A. A. (1978). Critical phenomena in the rheology of partially melted rocks. *Tectonophysics* **44**, 173–184.

Blake, D. H. & Page, R. W. (1988). The Proterozoic Davenport province, central Australia: regional geology and geochronology. *Precambrian Research* **40/41**, 329–340.

Brown, M. (1973). The definition of metatexis, diatexis and migmatite. *Proceedings of the Geological Association* **84**, 371–382.

Brown, M. (1994). The generation, segregation, ascent and emplacement of granite magma: the migmatite-to-crustally-derived granite connection in thickened orogens. *Earth-Science Reviews* **36**, 83–130.

Brown, M., Rushmer, T. & Sawyer, E. W. (1995). Introduction to special section: mechanisms and consequences of melt segregation from crustal protoliths. *Journal of Geophysical Research* **100**, 15551–15563.

Carrington, D. P. & Harley, S. L. (1995). Partial melting and phase relations in high-grade metapelites: an experimental petrogenetic grid in KFMASH system. *Contributions to Mineralogy and Petrology* **120**, 270–291.

Carson, C. J., Powell, R., Wilson, C. J. L. & Dirks, P. H. G. M. (1997). Partial melting during tectonic exhumation of a granulite terrane: an example from the Larsemann Hills, east Antarctica. *Journal of Metamorphic Geology* **15**, 105–126.

Chorlton, L. B. & Martin, R. F. (1978). The effect of boron on the granite solidus. *Canadian Mineralogist* **16**, 239–244.

Clarke, G. L., Collins, W. J. & Vernon, R. H. (1990). Successive overprinting granulite facies metamorphic events in the Anmatjira Range, central Australia. *Journal of Metamorphic Geology* **8**, 65–88.

Clarke, G. L., Daczko, N. R. & Nockolds, C. A. (2001). A method for applying matrix corrections to X-ray intensity maps using the Bence–Albee algorithm and Matlab. *Journal of Metamorphic Geology* **19**, 441–450.

Collins, W. J. & Vernon, R. H. (1991). Orogeny associated with anticlockwise P–T–t paths: evidence from low-P high-T metamorphic terranes in the Arunta Inlier, central Australia. *Geology* **19**, 835–838.

Collins, W. J. & Williams, I. S. (1995). SHRIMP ionprobe dating of short-lived Proterozoic tectonic cycles in the northern Arunta Inlier, central Australia. *Precambrian Research* **71**, 69–89.

Compston, D. M. (1995). Time constraints on the evolution of the Tennant Creek Block, northern Australia. *Precambrian Research* **71**, 107–129.

Ellis, D. J. & Obata, M. (1992). Migmatite and melt segregation at Cooma, New South Wales. *Transactions of the Royal Society of Edinburgh: Earth Sciences* **83**, 95–106.

Fitzsimons, I. C. W. (1996). Metapelitic migmatites from Brattstrand Bluffs, east Antarctica—metamorphism melting and exhumation of the mid crust. *Journal of Petrology* **37**, 395–414.

Gardien, V., Thompson, A. B., Gruijic, D. & Ulmer, P. (1995). Experimental melting of biotite + plagioclase + quartz ± muscovite assemblages and implications for crustal melting. *Journal of Geophysical Research* **100**, 15581–15591.

Grant, J. A. (1985). Phase equilibria in partial melting of pelitic rocks. In: Ashworth, J. R. (ed.) *Migmatites*. Glasgow: Blackie, pp. 86–144.

Grant, J. A. & Frost, B. R. (1990). Contact metamorphism and partial-melting of pelitic rocks in the aureole of the Laramie Complex, Morton Pass, Wyoming. *American Journal of Science* **290**, 425–472.

Greenfield, J. E. (1997). Migmatite formation at Mt Stafford, central Australia. Ph.D. thesis, University of Sydney, 231 pp.

Greenfield, J. E., Clarke, G. L., Bland, M. & Clark, D. C. (1996). In-situ migmatite and hybrid diatexite at Mt Stafford, central Australia. *Journal of Metamorphic Geology* **14**, 413–426.

Greenfield, J. E., Clarke, G. L. & White, R. W. (1998). A sequence of partial melting reactions at Mt Stafford, central Australia. *Journal of Metamorphic Geology* **16**, 363–378.

Hand, M. & Dirks, P. H. G. M. (1992). The influence of deformation on the formation of axial-planar leucosomes and the segregation of small melt bodies within the migmatitic Napperby Gneiss, central Australia. *Journal of Structural Geology* **14**, 591–604.

Harte, B., Pattison, D. R. M. & Linklater, C. M. (1991). Field relations and petrography of partially melted pelitic and semi-pelitic rocks. In: Voll, G., Töpel, J., Pattison, D. R. M. & Seifert, F. (eds) *Equilibrium and Kinetics in Contact Metamorphism, the Ballachulish Igneous Complex and its Aureole*. Berlin: Springer, pp. 182–210.

Holland, T. J. B. & Powell, R. (1996*a*). Thermodynamics of order–disorder in minerals. 1: symmetric formalism applied to minerals of fixed composition. *American Mineralogist* **81**, 1413–1424.

Holland, T. J. B. & Powell, R. (1996*b*). Thermodynamics of order–disorder in minerals. 2: symmetric formalism applied to solid solutions. *American Mineralogist* **81**, 1425–1437.

Holland, T. J. B. & Powell, R. (1998). An internally consistent thermodynamic dataset for phases of petrological interest. *Journal of Metamorphic Geology* **16**, 309–343.

Holtz, F. & Johannes, W. (1994). Maximum and minimum water contents of granitic melts: implications for chemical and physical properties of ascending magmas. *Lithos* **32**, 149–159.

Kerrick, D. M. (1990). *The Al_2SiO_5 Polymorphs*. *Mineralogical Society of America, Reviews in Mineralogy*, **22**, 406 pp.

Kerrick, D. M. & Speer, J. A. (1988). The role of minor element solid solution on the andalusite–sillimanite equilibrium in metapelites and peraluminous granitoids. *American Journal of Science* **288**, 152–192.

London, D., Morgan, G. B. & Wolf, M. B. (1996). Boron in granitic rocks and their contact aureoles. In: Anovitz, L. M. & Grew, E. S. (eds) *Boron: Mineralogy, Petrology and Geochemistry*. *Mineralogical Society of America, Reviews in Mineralogy* **33**, 299–325.

Mehnert, K. R. (1968). *Migmatites and the Origin of Granitic Rocks*. Amsterdam: Elsevier, 393 pp.

Motoyoshi, Y., Hensen, B. J. & Matsueda, H. (1990). Metastable growth of corundum adjacent to quartz in a spinel-bearing quartzite from the Archaean Napier Complex, Antarctica. *Journal of Metamorphic Geology* **8**, 125–130.

Pattison, D. R. M. & Harte, B. (1988). Evolution of structurally contrasting anatectic migmatites in the 3-kbar Ballachulish aureole, Scotland. *Journal of Metamorphic Geology* **6**, 475–494.

Powell, R. & Downes, J. (1990). Garnet porphyroblast-bearing leucosomes in metapelites: mechanisms and an example from Broken Hill, Australia. In: Ashworth, J. R. & Brown, M. (eds) *High Temperature Metamorphism and Crustal Anatexis*. London: Unwin Hyman, pp. 105–123.

Powell, R. & Holland, T. J. B. (1988). An internally consistent thermodynamic dataset with uncertainties and correlations: 3. Application, methods, worked examples and a computer program. *Journal of Metamorphic Geology* **6**, 173–204.

Powell, R. & Holland, T. J. B. (1993). On the formulation of simple mixing models for complex phases. *American Mineralogist* **78**, 1174–1180.

Powell, R. & Holland, T. J. B. (1999). Relating formulations of the thermodynamics of mineral solid solutions: activity modelling of pyroxenes, amphiboles and micas. *American Mineralogist* **84**, 1–14.

Renner, J., Evans, B. & Hirth, G. (2000). On the rheologically critical melt fraction. *Earth and Planetary Science Letters* **81**, 585–594.

Sandiford, M. & Powell, R. (1991). Some remarks on high temperature–low pressure metamorphism in convergent orogens. *Journal of Metamorphic Geology* **9**, 333–340.

Sandiford, M., McLaren, S. & Neumann, N. (2002). Long-term thermal consequences of the redistribution of heat-producing elements associated with large-scale granitic complexes. *Journal of Metamorphic Geology* **20**, 87–98.

Sawyer, E. W. (1987). The role of partial melting and fractional crystallization in determining discordant migmatite leucosome compositions. *Journal of Petrology* **32**, 701–738.

Sawyer, E. W. (1999). Criteria for the recognition of partial melting. *Physics and Chemistry of the Earth* **A24**, 269–279.

Sawyer, E. W. (2001). Melt segregation in the continental crust: distribution and movement of melt in anatectic rocks. *Journal of Metamorphic Geology* **19**, 291–309.

Sawyer, E. W., Dombrowski, C. & Collins, W. J. (1999). Movement of melt during synchronous regional deformation and granulite-facies anatexis, an example from the Wuluma Hills, central Australia. In: Castro, A., Fernandez, C. & Vigneresse, J. L. (eds) *Understanding Granites: Integrating New and Classical Techniques*. *Geological Society, London, Special Publications* **168**, 221–237.

Spear, F. S., Kohn, M. J. & Cheney, J. T. (1999). *P–T* paths from anatectic pelites. *Contributions to Mineralogy and Petrology* **134**, 17–32.

Stewart, A. J. (1981). *Reynolds Range Region, Northern Territory, 1:100 000 Geological Map Commentary*. Canberra, A.C.T.: Bureau of Mineral Resources, Geology and Geophysics, 22 pp.

Thompson, A. B. (1982). Dehydration melting of pelitic rocks and the generation of H_2O-undersaturated granitic liquids. *American Journal of Science* **282**, 1567–1595.

Vernon, R. H. (1982). Isobaric cooling of two regional metamorphic complexes related to igneous intrusions in southeastern Australia. *Geology* **10**, 76–81.

Vernon, R. H., Clarke, G. L. & Collins, W. J. (1990). Local, mid-crustal granulite facies metamorphism and melting: an example in the Mount Stafford area, central Australia. In: Ashworth, J. R. & Brown, M. (eds) *High Temperature Metamorphism and Crustal Anatexis*. London: Unwin Hyman, pp. 272–319.

Vielzeuf, D. & Holloway, J. R. (1988). Experimental determination of the fluid-absent melting relations in the pelitic system. *Contributions to Mineralogy and Petrology* **98**, 257–276.

Vigneresse, J. L., Barbey, P. & Cuney, M. (1996). Rheological transitions during partial melting and crystallization with application to felsic magma segregation and transfer. *Journal of Petrology* **37**, 1579–1600.

Vry, J., Compston, W. & Cartwright, I. (1996). SHRIMP II dating of zircons and monazites: reassessing the timing of high-grade metamorphism and fluid flow in the Reynolds Range, northern Arunta Block, Australia. *Journal of Metamorphic Geology* **14**, 335–350.

Warren, R. G. (1983). Metamorphic and tectonic evolution of granulites, Arunta Block, central Australia. *Nature* **305**, 300–303.

White, A. J. R., Chappell, B. W. & Cleary, J. R. (1974). Geologic setting and emplacement of some Australian Paleozoic batholiths and implications for intrusion mechanisms. *Pacific Geology* **8**, 159–171.

White, R. W. & Powell, R. (2002). Melt loss and the preservation of granulite facies mineral assemblages. *Journal of Metamorphic Geology* **20**, 621–632.

White, R. W., Powell, R. & Holland, T. J. B. (2001). Calculation of partial melting equilibria in the system Na_2O–CaO–K_2O–FeO–MgO–Al_2O_3–SiO_2–H_2O (NCKFMASH). *Journal of Metamorphic Geology* **19**, 139–153.

White, R. W., Powell, R. & Clarke, G. L. (2002). The interpretation of reaction textures in Fe-rich metapelitic granulites of the Musgrave Block, central Australia: constraints from mineral equilibria calculations in the system K_2O–FeO–MgO–Al_2O_3–SiO_2–H_2O–TiO_2–Fe_2O_3. *Journal of Metamorphic Geology* **20**, 41–55.

Wickham, S. M. (1987). Crustal anatexis and granite petrogenesis during low-pressure regional metamorphism: the Trois Seigneurs Massif, Pyrenees, France. *Journal of Petrology* **28**, 127–169.

Williams, I. S., Buick, I. S. & Cartwright, I. (1996). An extended episode of early Mesoproterozoic metamorphic fluid flow in the Reynolds Range, central Australia. *Journal of Metamorphic Geology* **14**, 29–47.

APPENDIX A: MINERAL ABBREVIATIONS

Biotite	bi	Muscovite	mu
Cordierite	cd	Orthopyroxene	opx
Garnet	g	Plagioclase	pl
Haematite	hem	Quartz	q
Ilmenite	ilm	Silicate melt	liq
K-feldspar	ksp	Sillimanite	sill
Magnetite	mt	Spinel	sp

APPENDIX B: MINERAL FORMULAE, COMPOSITIONAL VARIABLES AND ACTIVITY–COMPOSITION RELATIONSHIPS OF GARNET

The garnet model used in the THERMOCALC calculations, $X_2Y_3Si_3O_{12}$, involves Fe^{2+}, Mg and Ca exchange on the X site and Fe^{3+}, Al exchange on the Y site, and was modelled with the compositional variables

$$x_g = \frac{Fe^{2+}}{Fe^{2+} + Mg + Ca}$$

$$m_g = \frac{Mg}{Fe^{2+} + Mg + Ca}$$

$$f_g = \frac{Fe^{3+}}{2}.$$

The end-members are almandine (alm), pyrope (py), grossular (gr) and khoharite (kho; $Mg_3Fe_2^{3+}Si_3O_{12}$). The site distributions in garnet are

$$x_{Al,Y} = 1 - f_g$$

$$x_{Fe^{3+},Y} = f_g$$

$$x_{Fe^{2+},X} = x_g$$

$$x_{Mg,X} = m_g$$

$$x_{Ca,X} = 1 - x_g - m_g$$

with the end-member proportions being

$$p_{kho} = f_g$$

$$p_{alm} = x_g$$

$$p_{py} = m_g - f_g$$

$$p_{gr} = 1 - x_g - m_g.$$

The ideal mixing on sites expressions for the garnet end-members are:

$$a_{kho}^{ideal} = (x_{Mg,X})^3 (x_{Fe^{3+},Y})^2$$

$$a_{alm}^{ideal} = (x_{Fe^{2+},X})^3 (x_{Al,Y})^2$$

$$a_{py}^{ideal} = (x_{Mg,X})^3 (x_{Al,Y})^2$$

$$a_{gr}^{ideal} = (x_{Ca,X})^3 (x_{Al,Y})^2.$$

The non-ideal contributions were calculated using the symmetric formalism method outlined by Powell & Holland (1993, 1999) and Holland & Powell (1996*a*, 1996*b*).